STRUCTURAL AND THERMOCHRONOLOGIC EVIDENCE OF PALEOGENE-NEOGENE FAULTING AND EXHUMATION OF THE KLAMATH MOUNTAIN PROVINCE

By

Taylor C. Team

A Thesis Presented to

The Faculty of Humboldt State University

In Partial Fulfillment of the Requirements for the Degree

Master of Science in Environmental Systems: Geology

Committee Membership

Dr. Melanie Michalak, Committee Chair

Dr. Susan Cashman, Committee Member

Dr. Mark Hemphill-Haley, Committee Member

Dr. Margaret Lang, Program Graduate Coordinator

December 2021

ABSTRACT

STRUCTURAL AND THERMOCHRONOLOGIC EVIDENCE OF PALEOGENE-NEOGENE FAULTING AND EXHUMATION OF THE KLAMATH MOUNTAIN PROVINCE

Taylor C. Team

The Klamath Mountains Province (KMP), located at the southern end of the forearc of the Cascadia Subduction Zone, displays a distinct topographic and geologic signature. Compared to the forearc in the north, the KMP comprises Paleozoic-Mesozoic basement rocks with relatively high modern elevation and relief. This study investigates the pattern of rock cooling in the KMP by using thermochronology on plutons exhumed by faults and plutons outside of mapped faults. In this study I target three regions in the KMP: the Ashland pluton offset by the Siskiyou Summit fault in the northeast KMP, the Grayback pluton in the northwest KMP, and the China Creek pluton offset by the Browns Meadow fault in the southern KMP. Zircon (ZHe) and apatite (AHe) (U-Th)/He ages from these plutons record post emplacement cooling during the late Early Cretaceous and tectonic exhumation during the late Oligocene to early Miocene. Cooling ages from this study are compiled with available thermochronologic data to identify spatial and temporal patterns of exhumation. This comparison shows a late Oligocene to early Miocene cooling signal throughout the KMP, with the exception of a geographic cluster of late Eocene to early Oligocene AHe ages found in the south-central core of the KMP. This cluster of older cooling ages is bound by the Browns Meadow fault and La Grange

fault, indicating Tertiary faulting influenced exhumation in the southern KMP. However, the pervasive late Oligocene to early Miocene cooling signal suggests regional erosion is a more important factor influencing rock cooling than previously thought.

ACKNOWLEDGEMENTS

Special thanks to Dr. Melanie Michalak, Dr. Susan Cashman, and Dr. Mark Hemphill-Haley for the guidance and support during this project. Additional thanks to the rest of the Humboldt State University Geology department faculty for making my time at Humboldt State University over the past six years cherished.

This work was supported by a grant from the U.S. National Science Foundation (EAR 1758516). Thanks to Dr. Eric Kirby, Dr. Kevin Furlong, and Dr. Kirsty McKenzie for insight gained during research collaboration.

(U-Th)/He analyses were performed by University of Colorado Thermochronology Research and Instrumentation Lab (CU TRaIL). Thanks to Dr. Rebecca Flowers and Dr. James Metcalf.

TABLE OF CONTENTS

LIST OF TABLES

LIST OF FIGURES

INTRODUCTION

The Klamath Mountains Province (KMP) is located in the forearc of the southernmost Cascadia Subduction Zone, where modern plate boundary conditions transition from subduction to translation (Figure 1). Compared to the forearc in the north, the KMP displays high elevation and relief (e.g., Kelsey et al., 1994). Regional tectonic models on a larger scale have considered the KMP as a single rigid tectonic block, that has rotated during Eocene to Recent time, suggesting a lack of substantial internal Tertiary deformation (Magill and Cox, 1981; Mankinen et al., 1989; Wells et al., 1998; McCaffrey et al., 2007). However, at the smaller scale, Tertiary faulting has been identified and investigated over the past six decades, in the southern KMP (Irwin, 1960; Davis, 1968; Schweikert and Irwin, 1989), the northeast boundary of the KMP (Wells, 1956), and more recently in the northwestern KMP (von Dassow, 2018), providing some evidence of internal deformation. In this study, I evaluate major Tertiary faults in a broader context on a first-order attempt to establish a cohesive timeline of Tertiary tectonism in the KMP, and target specific faults using geochronologic dating methods in order to constrain timing and magnitude of slip.

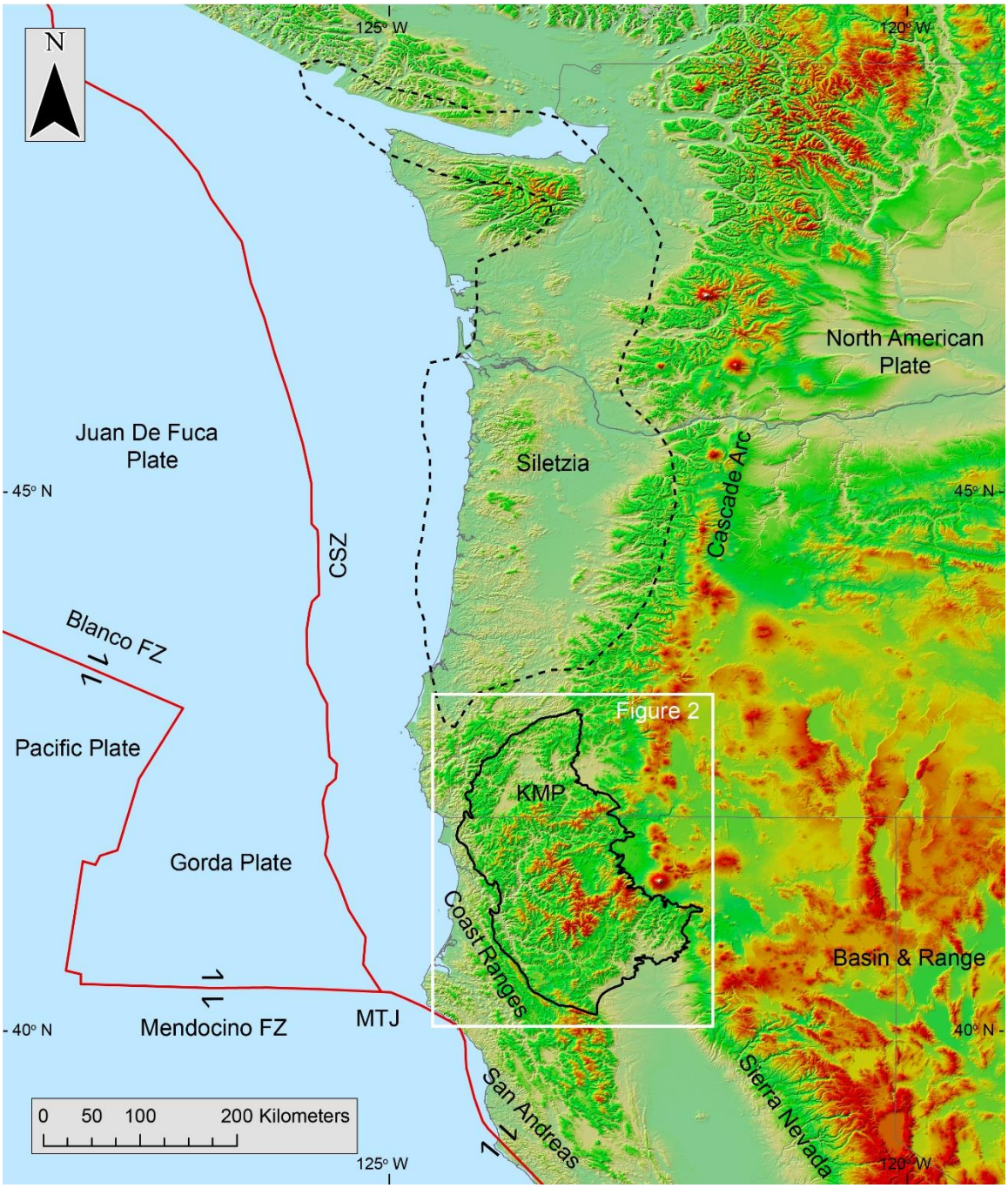

Figure 1. Regional map displaying the current tectonic setting of the Pacific Northwest. Tectonic plates, significant geological provinces and plate boundaries (U.S. Geological Survey and ESRI, 2010) are labeled. The outline of the Klamath Mountain Province (KMP) is digitized from Irwin (1994). The outline of the Siletzia province is digitized from Wells et al. (2014) and is shown by the dashed line. The hillshade background was constructed in ArcMap from 30 m SRTM DEM data. CSZ=Cascadia Subduction Zone, MTJ=Mendocino Triple Junction.

Overall, while certain individual Tertiary faults in the KMP are thoroughly characterized, establishing timing and style of Tertiary faulting more broadly is not well understood. The La Grange fault (LGF) is a known extensional fault, the Siskiyou Summit fault (SSF) is mapped as a high angle normal fault, and the Browns Meadow Fault (BMF) is a high angle fault that may be extensional. Previous work has helped constrain the timing of southern KMP extensional faulting, i.e., the LGF, to have occurred between ~45-15 Ma (Batt et al., 2010a; Piotraschke et al., 2015; Team, 2018, Puleri et al., 2019) with an extent of ~60 km southward displacement through the shallow upper crust (Schweikert and Irwin, 1989; Cashman and Elder, 2002; Cashman and Cashman, 2006). NE-SW trending, syntectonic grabens containing the Oligocene-Miocene Weaverville Formation provide evidence of extension in the southern KMP (Phillips and Aalto, 1989). Besides recent studies focusing on the LGF, limited work other than detailed mapping during the 1960s-1980s has been done to address other similarly-aged faults located in the central and northern KMP (Figure 2A).

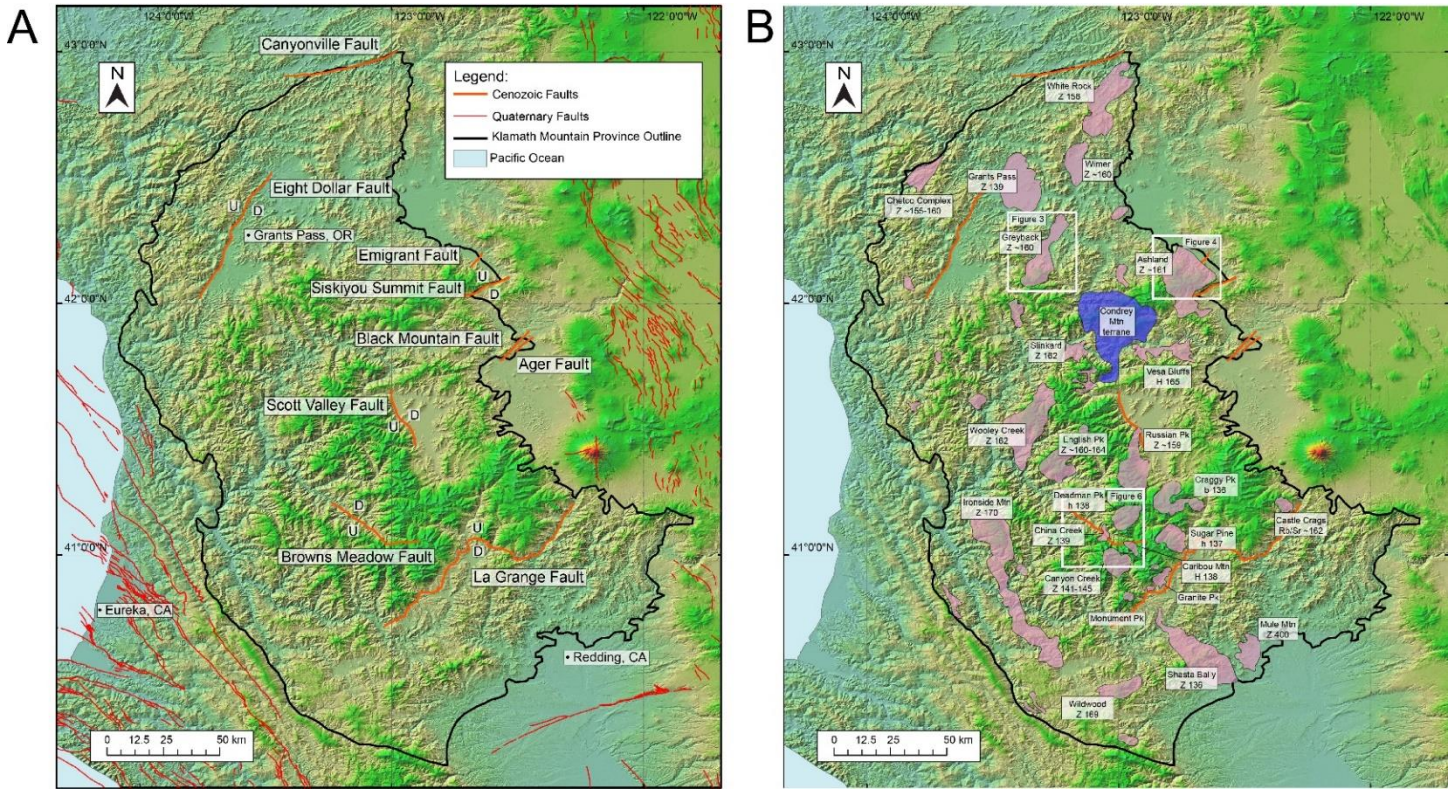

Figure 2. A) Hillshade basemap constructed in ArcMap from 30 m SRTM DEM data displaying the traces of Cenozoic-aged faults within the KMP in orange, and Quaternary faults outside the KMP in red. Cenozoic-aged faults are labeled by name and have thicker lines while Quaternary faults are unlabeled and have thinner lines. U=Up and D=Down, denoting the upthrown and downthrown block for KMP faults, where known. KMP faults and the KMP outline were digitized from Irwin (1994). Quaternary faults are from the national database of Quaternary faults (U.S. Geological Survey and California Geological Survey, 2020). B) Hillshade basemap displaying plutons (pink, labeled), Cenozoic faults (orange), and Condrey Mountain terrane (blue) within the KMP. Plutons associated crystallization ages, and the Condrey Mountain terrane were digitized from Irwin and Wooden (1999). Z=U-Pb zircon age, H=Ar-Ar hornblende age, where unlisted no age is known/published. Faults and the KMP outline (black) were digitized from Irwin (1994). White boxes represent locations of figures 3,4, and 6. The hillshade background was constructed in ArcMap from 30 m SRTM DEM data.

The primary objectives of this study are to 1) quantify the magnitude and timing of Tertiary to Recent faulting and crustal exhumation in the northern KMP using thermochronology, 2) compare to detachment-driven exhumation in the southern KMP and 3) compile all regional thermochronologic data to analyze spatial and temporal patterns of exhumation occurring throughout the province. The location and orientation of Tertiary faults as well as geologic and thermal constraints on their activity may inform the spatial distribution of deformation in the KMP through time. Low temperature thermochronology can be utilized to constrain fault activity by tracking the exhumation of rocks through the upper crust. Cooling ages of bedrock samples from plutons displaced by or proximal to faults may indicate when fault activity began and at what rate, as the cooling history of a pluton can be used as a proxy for the timing and duration of fault-driven exhumation (Holm et al., 1992; Foster and John, 1999; Reiners and Brandon, 2006). Plutonic rocks are targeted because unlike much of the mafic to ultramafic KMP basement, granodioritic and tonalitic plutons yield high quality accessory minerals appropriate for thermochronologic methods.

To investigate the role of Tertiary faulting in crustal exhumation of the KMP, we sample a geographic range of plutons within the province. The Ashland pluton and China Creek pluton are ideal locations for this approach because they are bisected by Tertiary faults found in the northeastern and central KMP and timing and duration of slip on these faults are not yet constrained by thermochronologic methods. The Grayback pluton and Ironside Mountain Batholith, both outside the range of known Tertiary faults, provide controls to compare the exhumation patterns of plutons driven by tectonic activity versus

regional factors. We then compare these new data to the entire thermochronology dataset of the KMP in order to identify spatial and temporal patterns of exhumation.

Tectonic Setting

Presently, the KMP is located at the southern end of the CSZ forearc (Figure 1). To the south of the KMP, the plate boundary shifts from subduction to San Andreas system translation at the Mendocino Triple Junction. To the north of the Mendocino Triple Junction, subduction under the North American plate transitions from subduction of the younger, more buoyant Gorda plate to the older, more rigid Juan De Fuca plate at the Blanco Fracture Zone (Figure 1). The Oregon coastal block lies inboard of the Blanco Fracture Zone in the forearc directly to the north of the KMP and consists of accreted oceanic crustal rocks, e.g., Siletzia, that have rotated clockwise at a rate of 1.5^{o}/m.y. and migrated northward during Cenozoic time (Magill et al., 1982; Wells et al., 1998). The active Cascade volcanic province lies to the northeast of the KMP. The southern Cascade Range, directly to the east of the KMP, marks the transition between northwest-southeast dextral shear associated with the Walker Lane to east-west extension observed in the Cascade arc to the north (Blakely et al., 1997).

Despite being located in the center of such a complex tectonic setting, the KMP does not contain many recognized Quaternary faults (Figure 2A). Recent studies looking at geodetic data show how upper plate structure and lithologies in the Cascadia forearc have contributed to interseismic uplift and coseismic subsidence rates (Shmalzle et al., 2014; Materna et al., 2019). In central Cascadia, interseismic uplift and coseismic

subsidence rates are significantly reduced, which can be attributed to enhanced creep associated with interactions between the subduction zone fault interface and the Siletzia province in the upper plate (Schmalzle et al., 2014). In southern Cascadia, variations in interseismic deformation data, previously assumed to be constant, are attributed to changes in the amount of coupling that appear to vary with proximal M>6.5 earthquakes (Materna et al., 2019). Deciphering the amount of coupling, slow slip, and associated deformation occurring within a subduction zone is an exceptionally difficult problem that has been a recent focus for geodynamicists studying Cascadia. Understanding long term uplift rates in the forearc, with the aid of methods like thermochronology, used in this study, may help contribute to this understanding.

The KMP was formed by terrane accretion and arc magmatism during the Paleozoic and Mesozoic subduction of oceanic lithosphere under the North American plate (Irwin, 1960; Irwin, 1972).The upper plate crustal structure of the KMP consists of a series of Paleozoic to Jurassic accreted terranes that young to the west and are separated by eastward-dipping thrust faults (Irwin, 1960; Irwin, 1972; Irwin, 1985). These terranes have been divided into punctuated accretionary episodes occurring from the Late Silurian to Early Cretaceous (Irwin and Wooden, 1999). The terranes are intruded by numerous calc-alkaline plutons that are classified as preaccretionary or accretionary depending on whether they intruded into the host terrane before or after the terrane accreted to the continent (Irwin, 1960; Irwin, 1985; Barnes et al., 1992; Irwin and Wooden, 1999). Terrane accretion was completed during the Nevadan Orogeny (155-135 Ma)(Harper et al., 1994). KMP plutons have been organized into plutonic suites dependent on isotopic

composition and U-Pb zircon ages (e.g., Barnes et al., 1992; Irwin and Wooden, 1999; Allen and Barnes, 2006). The majority of KMP pluton ages range from 135-175 Ma, with the exception of a few, localized 400-430 Ma gabbroic to ultramafic plutons found in the eastern KMP (Allen and Barnes, 2006) (Figure 2B). The Ashland pluton (160-161, 152-156 Ma)(crystallization age range) and Grayback pluton (157-160 Ma) both belong to the Wooley Creek Suite, the China Creek pluton (149 Ma) belongs to the Western Klamath suite, and the Ironside Mountain Batholith (170 Ma) is not categorized due to large size and composition (Allen and Barnes, 2006; Barnes et al., 1995; Gribble et al., 1990; Irwin and Wooden, 1999; Yule et al., 1996). Geobarometric and petrologic studies on central KMP plutons, e.g. Russian Peak, Wooley Creek, constrain emplacement depths to 10-12 km (Barnes et al., 1986a; Cotkin and Medaris, 1993).

After emplacement of plutons during the Nevadan orogeny and accretion ending in the Early Cretaceous with the Pickett Peak episode (Irwin and Wooden, 1999), evidence suggests the KMP underwent burial and exhumation, apparent by overlapping, unconformable deposition of the Cretaceous Hornbrook Formation on the eastern margin of KMP basement rocks (Nilsen, 1984) and the mapped remnants of the Great Valley Sequence (Sliter et al., 1984). The Hornbrook Formation consists of transgressive nearshore and shelf deposits containing significant KMP detritus, indicating portions of the KMP were at sea level and other areas were actively eroding during middle to late Cretaceous (Nilsen, 1984; Sliter et al., 1984). Vitrinite reflectance values from the Hornbrook Formation show sedimentary thicknesses reached up to 5 km, suggesting the Hornbrook basin was likely much larger than the remnants exposed today (Batt et al.,

2010b). Correlations between the KMP and Sierra Nevada indicate the Hornbrook Formation was likely part of a much larger depositional system formed during the separation episode where the Sierra Nevada block rifted from the KMP during the Early Cretaceous (Irwin, 2003; Batt et al., 2010b). Changes in detrital zircon distributions between the lower and upper Hornbrook Formation show a shift in provenance from the KMP and Blue Mountains to the Sierra Nevada Batholith from the middle to late Cretaceous, suggesting the KMP went from actively eroding to a region of subsidence and sedimentation during this time period (Surpless and Beverly, 2013; Surpless, 2015). Ar^{40}-Ar^{39} and zircon fission track ages from plutons in the western KMP provide additional evidence for an episode of uplift and active erosion during the late Early Cretaceous, followed by quiescence until accelerated cooling related to widespread Laramide uplift occurred during Campanian time (Batt et al., 2010b).

Between 56-49 Ma, the Siletzia microplate was accreted to North America, reorganizing the plate boundary to form the modern Cascadia Subduction Zone (Schmandt and Humphreys, 2011; Wells et al., 2014). The accretion of Siletzia, a large igneous province, occurred to the north of the KMP within the Columbia Embayment. Accretion was completed by 51-49 Ma, marked by deposition of the onlapping Tyee Formation (Wells et al., 2014). Previous studies have identified the accretion of Siletiza as a potential driver of Tertiary extension in the southern KMP (Piotraschke et al., 2015), however, the mechanism and timing surrounding how this occurred is still unclear. Between 42-34 Ma, the Oregon forearc experienced renewed magmatism with the Tillamook magmatic episode, including basalt-rhyolite magmatism, regional dike

swarms, and margin-parallel extensional tectonics (Wells et al., 2014). The mechanisms generating Siletzia and the reorganization of the plate boundary are debated, and center around interactions with the Yellowstone hotspot (Wells et al., 2014; Stern and Dimitru, 2019). Stern and Dimitru (2019) developed a plume-induced subduction initiation hypothesis to explain how oceanic lithosphere could rupture after interacting with a mantle plume, followed by the initiation of a new subduction zone. Piotraschke et al. (2015) hypothesize Siletzia accretion and subsequent reorganization of a subduction zone with newly oblique convergence prompted extensional deformation to the south in the KMP during Tertiary time.

Tertiary faulting and exhumation

Extensional fault-driven crustal exhumation is recorded in the KMP during Tertiary time along the La Grange fault (LGF) (Schweikert and Irwin, 1989). However, some Tertiary faults within the KMP display separation associated with strike-slip mechanics, such as the Canyonville Fault (Perttu, 1976), and others have geometries that permit normal or reverse motion, such as the Browns Meadow fault and Eight Dollar fault (Davis, 1968; von Dassow, 2018). Additional faults may exist that have yet to be identified due to a lack of available field relationships, as there are few Tertiary sedimentary units within the KMP as well as the presence of volcanic cover. Although the Tertiary rock record is poorly preserved in these regions, there is evidence for the activity of numerous Tertiary faults.

Previous work in the southern KMP has primarily focused on constraining the activity of the LGF, a low angle SE-NW striking detachment fault (Schweikert and Irwin,

1989). Observations and petrologic investigations of cataclasite and ultracataclasite associated with the LGF detachment indicate prolonged and brittle deformation in the shallow crust, exhuming footwall rocks and transporting hanging wall rocks southward up to 60 km (Cashman and Elder, 2002; Cashman and Cashman, 2006). Batt et al. (2010a) and Piotraschke et al. (2015) utilized low temperature thermochronology to constrain the timing of LGF activity, assuming plutons located in the footwall of the LGF were brought to the surface solely by detachment-driven exhumation. Apatite (U-Th)/He (AHe) cooling ages from footwall plutons range from 15-40 Ma, with the youngest AHe ages found closest to the LGF trace (Batt et al., 2010a, Piotraschke et al., 2015; Team, 2018; Puleri et al., 2019), suggesting the LGF was active and exhibiting southward transport of hanging wall rocks and upper crustal exhumation through this time.

Bedrock samples collected in a vertical transect of the Canyon Creek pluton, located in the southern KMP within the footwall of the LGF, show six AHe mean ages ranging from 24.7-15.2 Ma (Team, 2018). These data yield exhumation rates derived from the cooling age-elevation relationship method of 0.14 km/m.y. from 24.7-15.2 Ma and 0.19 km/m.y. from 15.2 Ma-present (Team, 2018). The Granite Peak pluton is located just south of the Canyon Creek pluton, closest to the trace of the LGF (Figure 2B). Granite Peak AHe ages range from 19.8-14.6 Ma, producing an age-elevation relationship exhumation rate of 0.21 km/m.y. during this time period (Puleri et al., 2019). The oldest AHe ages within the KMP range from 40-30 Ma and are found in central KMP plutons, i.e., Deadman Peak, Craggy Peak (Batt et al., 2010a; Piotraschke et al., 2015).

In the forearc and Cascade Range of Oregon and Washington, thermochronology records younger exhumation compared to the KMP. ZHe and AHe ages from the Olympic Mountains record exhumation rates starting at 0.25 km/m.y. at 18 Ma, followed by increases in exhumation rates at 5 Ma to the present up to 0.9 km/m.y. (Michel et al., 2018). The majority of AHe ages from the Olympic Mountains range from 15 to 1.5 Ma (Michel et al., 2018). AHe ages from the west flank of the Washington Cascade Range record accelerated late Miocene cooling with AHe ages ranging from 12-6 Ma and corresponding exhumation rates between 0.5-1.0 km/m.y. (Reiners et al., 2002). However, AHe ages from the east flank of the Washington Cascade Range record prolonged exhumation from 60 to 18 Ma at rates between 0.15-0.25 km/m.y. (Reiners et al., 2002), similar to the rates observed in south-central KMP plutons. Detrital bedrock AHe ages from the Chumstick Basin, also located on the east flank, record slightly younger exhumation driven through the late Miocene with AHe ages ranging from 17-11 Ma (Enkelmann et al., 2015). Enkelmann et al. (2015) suggest erosional exhumation of the Chumstick Basin was driven by reactivated faults responding to a Miocene switch to north-south compressional tectonics in the Washington Cascade Range. AHe ages from six catchments along the Cascade arc from Oregon to southern Washington show similar ages ranging from 23-8 Ma, with cooling attributed to tectonic uplift occurring earlier in Oregon and more recently in Washington (Pesek et al., 2020). The southernmost site from Pesek et al. (2020) is located 75 km north of the Ashland pluton (this study) and contains AHe ages ranging from 22-17.8 Ma.

Geomorphic and sedimentological observations of the most recent exhumation after LGF activity in the south-central KMP include determining timing of marine to terrestrial deposition of the Wimer Formation in the northwest KMP and the development of low relief, elevated surfaces proximal to the coast. The Wimer Formation is a late Miocene to early Pliocene shallow marine sedimentary deposit located on uplifted plateaus in the coast ranges boarding the westernmost KMP (Maxson, 1933; Irwin, 1966). After deposition of the Wimer Formation and return to shallow marine conditions, the western KMP and coast ranges were thought to have been reduced in elevation as a regional erosional surface was formed (Diller, 1902; Aalto, 2006). The underlying Wimer Formation provides evidence that the regional erosional surface was at sea level near the early Pliocene and uplifted during Pleistocene-Holocene time, implying regional uplift of up to 1220 m during the last 5 Ma, at a rate of approximately 0.24 km/Ma (Aalto, 2006).

Lack of cooling ages from plutons within the KMP but outside of the footprint of the LGF, limits the ability to determine whether the exhumation signal in the south-central KMP is reflective of a regional signal or constricted to the LGF region. The Grayback pluton and Ironside Mountain Batholith are selected for thermochronology as they are not clearly offset or exhumed by faults, therefore thermochronologic data from these plutons may assess rates and timing of regional exhumation that is not locally affected by faults. The Grayback pluton (Figure 3) can provide a control to compare the fault-driven exhumation signal from the northern Ashland pluton. The Ironside Mountain Batholith can act as a control to compare fault-driven exhumation of the China Creek, and other southern Klamath plutons, e.g., Canyon Creek, to a regional erosional

exhumation signal. Utilizing structural analysis and thermochronology, two major faults examined here are the Siskiyou Summit Fault (SSF) and Browns Meadow Fault (BMF).

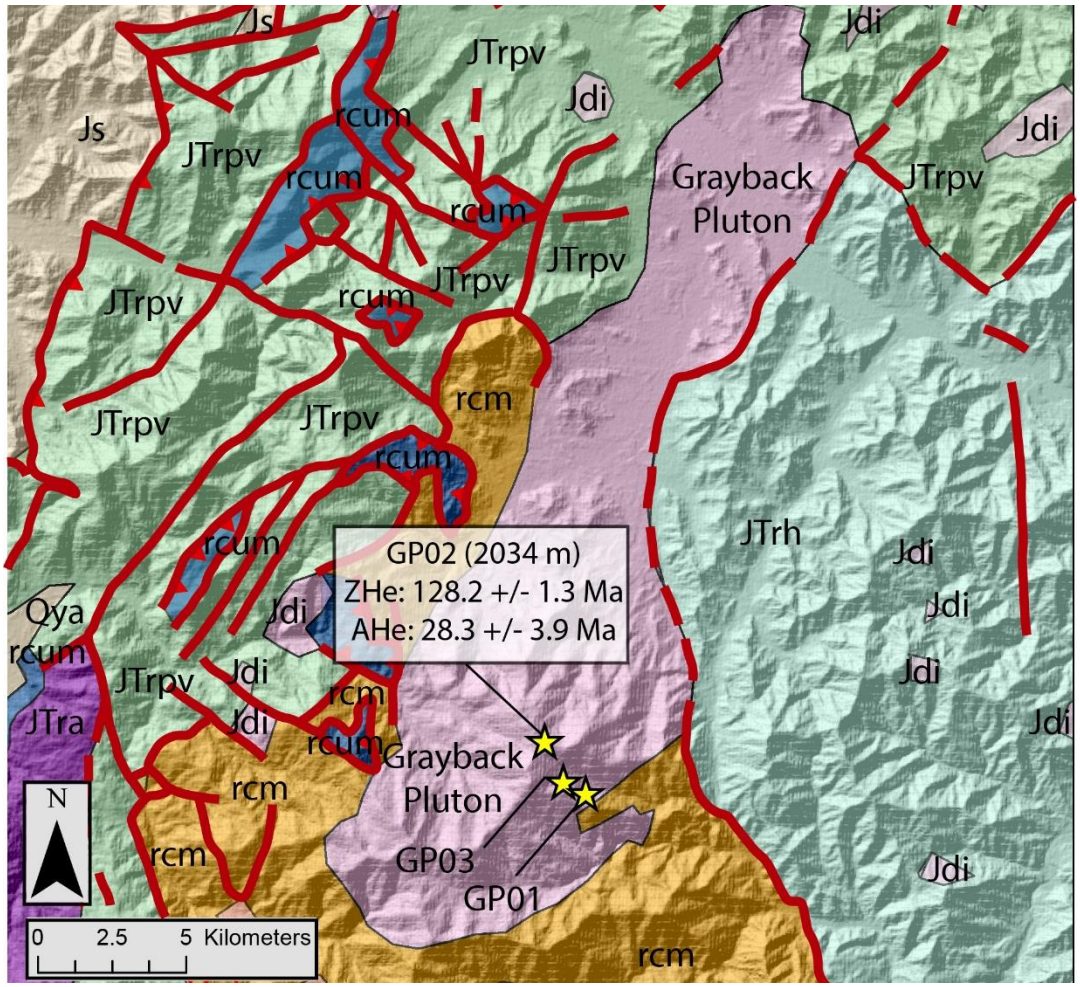

Figure 3. Bedrock geology map of the Grayback pluton area. Thick red lines denote the trace of faults, with teeth marks indicating the upper plate of thrust faults, and dashed lines showing where fault is inferred. Stars show locations of bedrock samples for AHe thermochronology from the Grayback pluton. The following is the key for the bedrock geology symbols in decreasing age order; Hayfork Terrane: JTra=Andesitic and dacitic volcanic rocks, JTrh=Hornblende volcanic rocks, JTrpv=Pyroxene volcanic rocks; Rattlesnake Creek Terrane: rcum=Serpentinized ultramafic rocks, rcm=mélange; Western Klamath Terrane: Js=Sedimentary rocks; plutonic rocks: Jdi=diorite; Qya=younger alluvial deposits. The geologic map was digitized from the Geologic Map of the Klamath Mountains (Irwin, 1994). The hillshade background was constructed in ArcMap from 30 m SRTM DEM data.

Siskiyou Summit fault (SSF)

The SSF is a normal fault, located in the northeastern KMP, that displaces Cretaceous-Tertiary sedimentary rocks and bounds the northern edge of a major graben (Bestland, 1987). Numerous NE trending faults are mapped to the north and south of the SSF, over a geographic extent of ~30 km (Wells, 1956). The SSF strikes N65E, dips 65 degrees SE and has a trace of >24 km, displacing the Cretaceous Hornbrook Formation by 11.3 km of right-lateral separation, measured by the contact marker between the Hornbrook Formation and Umpqua Formation (Wells, 1956) (Figure 4). Utilizing the dips of bedding of offset units, we estimate using trigonometry a normal separation of ~ 6 km (Figure 5). Offset of the Hornbrook Formation limits earliest fault activity to the late Cretaceous, with deposition ending in the Maastrichtian (Surpless and Beverly, 2013). Lack of offset within the upper Colestin Formation, which overlies offset units, indicates fault activity ceased by 27 Ma (Vance, 1984; Bestland, 1987). Using these geologic constraints we estimate the SSF was active between ~65-27 Ma. However, northward thickening of a subunit of the upper Colestin Formation, deposited after deposition of a 30 Ma basalt flow (Sutter, 1978) and prior to SSF activity ending, records evidence the SSF was active in the later end of the bracketed time window (Bestland, 1987). In addition, observations of downfaulting of the Siskiyou Pass area during deposition of the upper Colestin formation indicates a potential reversal of slip of the SSF towards the end of its activity (Bestland, 1987).

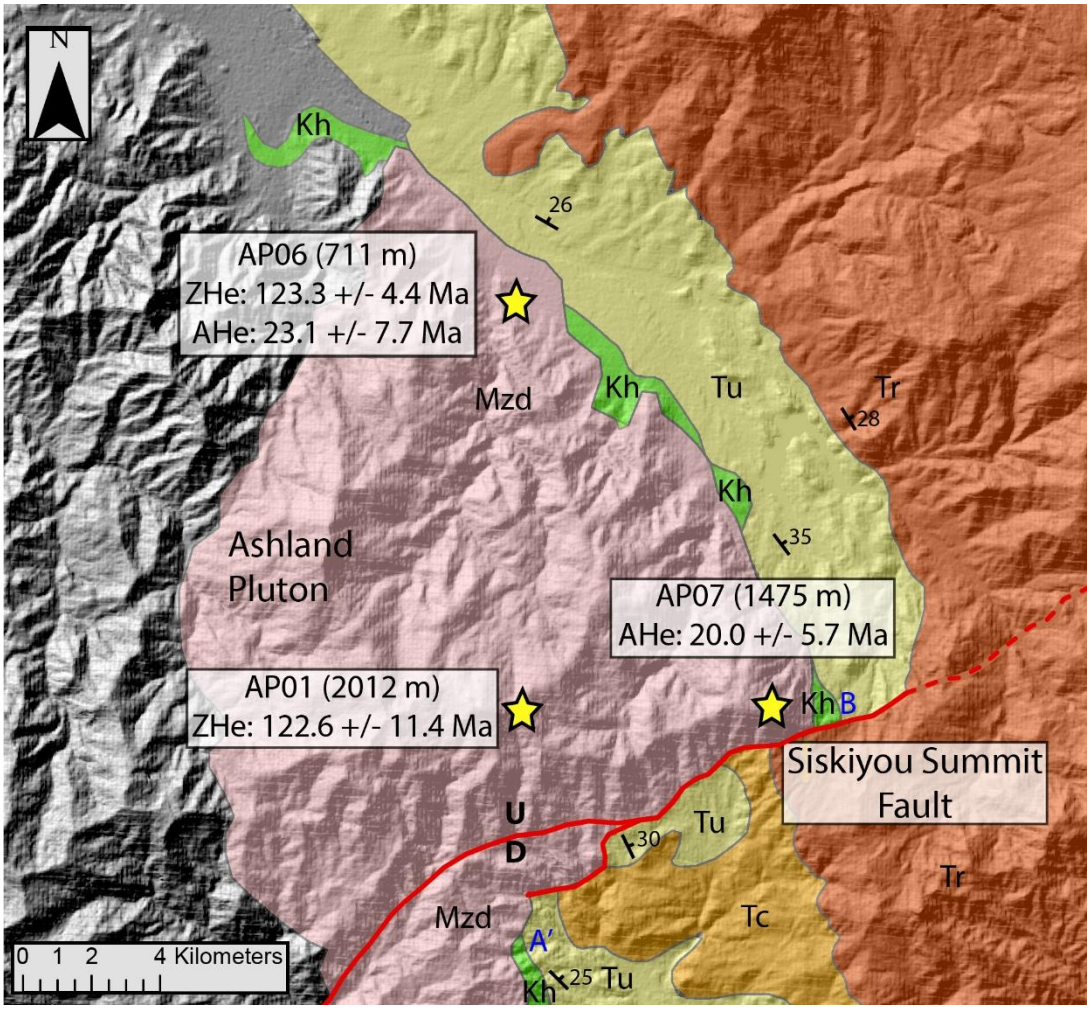

Figure 4. Bedrock geology map of the Ashland pluton (pink) and offset from the Siskiyou Summit Fault (SSF). The thick red line shows the SSF trace with U denoting the upthrown block and D denoting the downthrown block. The dashed red line denotes where the fault contact is concealed. A' and B (blue) correlate to the block diagram shown in Figure 7. Yellow stars indicate the location of bedrock samples from this study that correlate to zircon (U-Th)/He (ZHe) and apatite (U-Th)/He (AHe) cooling ages shown in white boxes. The geologic map and measure bedding attitudes (hatched black lines) were digitized from Wells (1956). The following is the key for the bedrock geology symbols in decreasing age order: Mzd=Mesozoic diorite, Kh=Hornbrook Formation, Tu=Umpqua Formation, Tc=Colestin Formation, Tr=Roxy Formation. The hillshade background was constructed in ArcMap from 30 m SRTM DEM data.

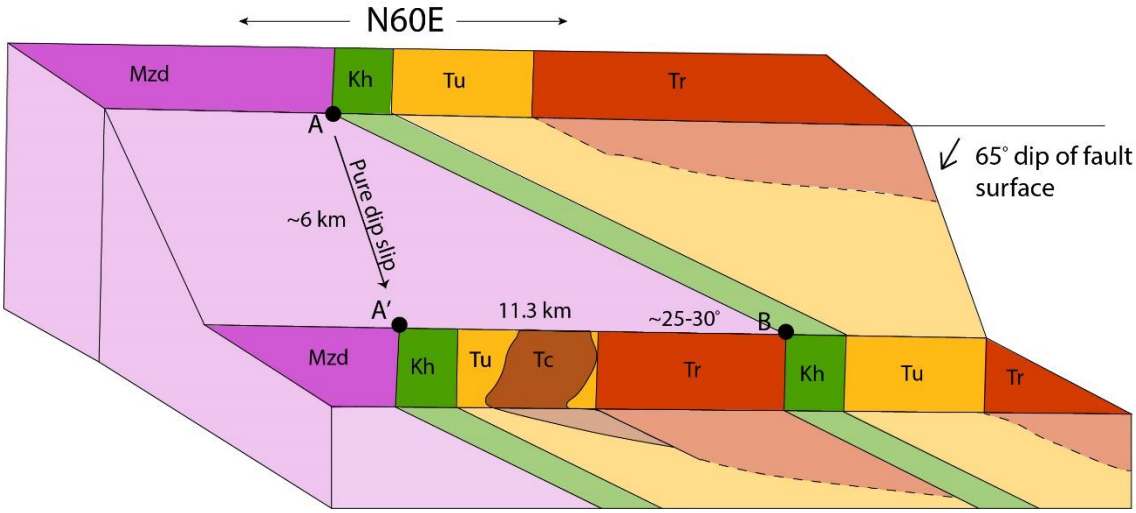

Figure 5. Simple geometric model of the Siskiyou Summit Fault (SSF), drawn along strike of the SSF with assumed pure dip-slip kinematics. Bold colors show surface geology, transparent colors indicate geology inferred at depth, based on measured attitudes on the surface. Assuming a 65° dip of the fault surface, pure dip slip, and using a range of bedding dips between ~25-30°, the SSF displaces the Hornbrook Formation by ~6 km. The following is the key for the bedrock geology symbols in decreasing age order: Mzd=Ashland pluton, Kh=Hornbrook Formation, Tu=Umpqua Formation, Tc=Colestin Formation, Tr=Roxy Formation.

The SSF also bisects the Jurassic Ashland pluton, with the majority of the pluton exposed in the footwall. Based on the ~25-30° dips of the onlapping Hornbrook Formation, as well as petrologic observations on zonation, the Ashland pluton appears to have tilted to the east at least 25° since emplacement, exposing 7 to 8 km of structural relief (Wells, 1956; Barnes et al., 1986b). The tilting of the Ashland pluton and proximal fault activity have been suggested to be related to differential uplift in the west associated with Neogene doming of the Condrey Mountain area (Mortimer and Coleman, 1985; Barnes et al., 1986b), however, Neogene-aged doming is challenged by more recent thermochronologic data by Piotraschke et al. (2015). Tilting of the Ashland pluton presents a challenge to interpreting paleomagnetic rotation data, as the Ashland pluton does not display clockwise rotation observed in other north-central KMP plutons, i.e.,

Grayback and Grants Pass (Schulz, 1983). Other paleomagnetic studies on Cretaceous to Tertiary sedimentary deposits within the KMP show 11.5^{o} +/- 15.8^{o} of clockwise rotation since Cretaceous time (Mankinen and Irwin, 1982). These values are much less than rotation observed in the Oregon Coast Range, suggesting the KMP and Oregon Coast Range did not act as a single rigid block during Tertiary time and that the Oregon Coast Range block responded differently to the collision of Siletzia compared to the KMP (Mankinen and Irwin, 1982).

Cooling ages derived from bedrock samples of the Ashland pluton place further constraints on the timing of fault activity, may provide insight into proposed tilting and uplift, as well as test the proposed hypothesis that SSF activity produced ~6 km of normal separation. Exhumation rates derived from the cooling age-elevation transect can be viewed as a proxy for slip rate, as the fault may have contributed to cooling of the Ashland pluton as it exhumed the pluton through the upper crust.

Browns Meadow fault (BMF)

The BMF is located in the south central KMP, has a trace length of ~37 km, and bisects the Jurassic China Creek pluton with apparent motion of down to the north and up to the south (Davis, 1968; Irwin, 1994) (Figure 6). This relative motion is opposite to that of the LGF located to the south of the BMF, where footwall rocks of the LGF are exhumed to the north and hanging wall rocks are transported to the south (Figure 2A). The BMF displaces late Paleozoic to Jurassic rocks of the North Fork Terrane (Irwin, 1994), with the youngest unit displaced being the China Creek pluton (149 Ma U-Pb zircon age; Irwin and Wooden, 1999). The Siskiyou thrust fault provides a marker for

offset estimation as it is found on either side of the BMF (Figure 7). The BMF strikes ~N60W for the majority of its length, then is mapped to change orientation to ~EW just east of the China Creek pluton (Figure 6). The lack of Tertiary-recent units in this area presents a challenge to constraining the timing of fault activity. Cooling ages of bedrock samples from the China Creek pluton in the footwall and hanging wall of the BMF test the hypothesis that fault-driven exhumation occurred during Tertiary time.

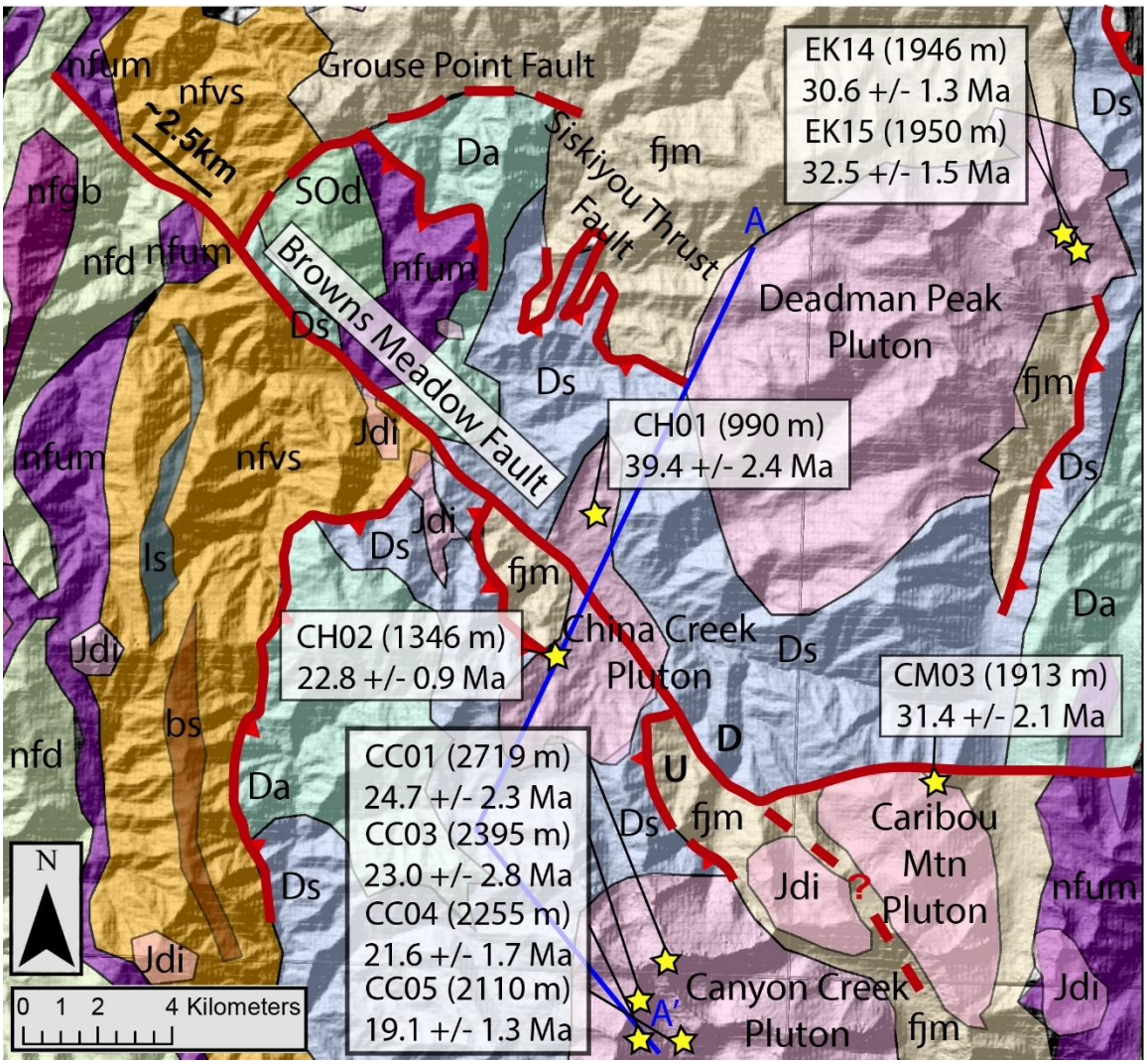

Figure 6. Bedrock geology map and offset from the Browns Meadow Fault (BMF). Thick red lines denote the trace of faults and are dashed where inferred, with U symbolizing up and D symbolizing down for relative motions of faulting of the BMF; and teeth marks denoting the upper plate of thrust faults. The cross section line for Figure 5 is shown by the blue line from A to A'. Yellow stars indicate the location of bedrock samples that correlate to apatite (U-Th)/He cooling ages (AHe) shown in the white boxes. AHe data are from various sources; CM03 (Piotraschke et al., 2015), EK14 and EK15 (Batt et al., 2010a), CH01 and CH02 (this study), CC01, CC03, CC04, and CC05 (Team, 2018). Prominent Jurassic-Cretaceous plutons (in pink) and faults are labeled by name. The following is the key for the bedrock geology symbols in decreasing age order; Eastern Klamath Terrane: SOd=Duzel Phyllite; Central Metamorphic Terrane: Ds=Salmon Schist, Da=Abrams Schist; Fort Jones Terrane: fjm=metasedimentary and metavolcanics rocks; North Fork Terrane: nfum=ultramafic rocks, nfgb=gabbro, nfd=diabase and basalt, nfvs=volcanic and sedimentary rocks; Rattlesnake Creek Terrane: ls=minor limestone; Condrey Mountain Terrane: bs=blueschist; plutonic rocks: Jdi=diorite. The geologic map was digitized from Irwin (1994). The hillshade background was constructed in ArcMap from 30 m SRTM DEM data.

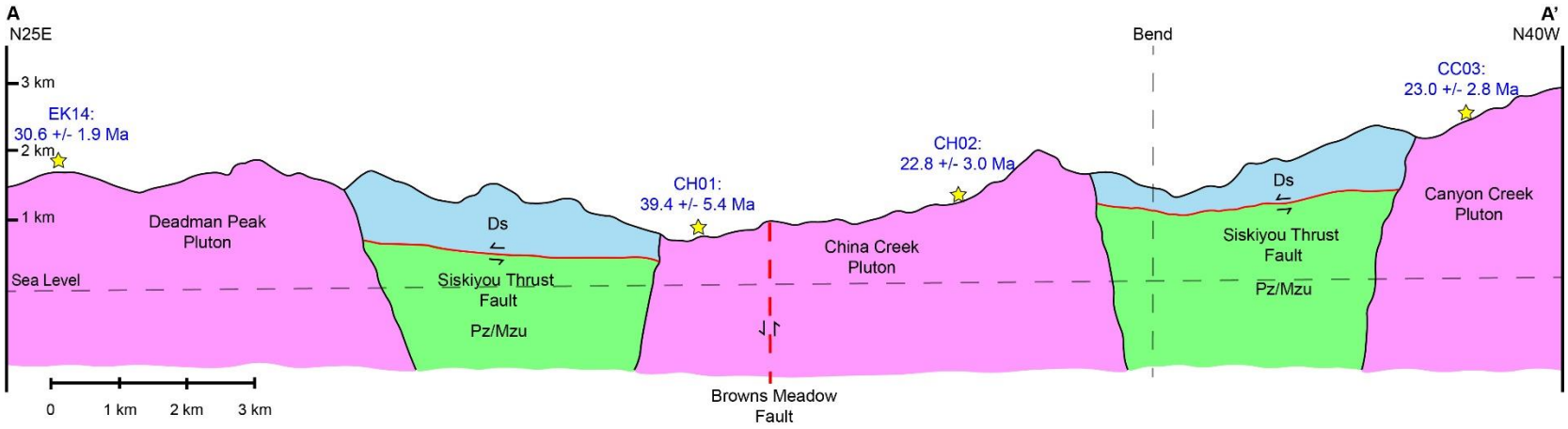

Figure 7. A to A' cross section showing vertical separation of the Browns Meadow Fault (BMF) (dashed red line). Apatite (U-Th)/He (AHe) samples and ages from plutons (pink) are shown in blue and sample locations and elevations are shown by yellow stars, projected onto the cross section line. AHe data are from various sources; EK14 (Batt et al., 2010a), CH01 and CH02 (this study), and CC03 (Team, 2018). The "Bend" dashed line denotes where the cross section line changes direction from N25E to N40W. The following is the key for bedrock geology symbols in decreasing age order; Ds=Salmon Schist (blue); Pz/Mzu=Paleozoic/Mesozoic Undivided (green).

METHODS

Eight bedrock samples from the Ashland pluton, three bedrock samples from the Grayback pluton, two bedrock samples from the China Creek pluton, and one bedrock sample from the Ironside Mountain batholith were collected with use of rock hammer, sledge, and chisel, and stored in plastic bags for processing. The locations of the samples were recorded with hand-held GPS and logged in a field notebook and Excel spreadsheet (Table 1).

Standard mineral separation techniques were utilized to isolate apatite and zircon for (U-Th)/He analyses. These techniques included crushing, milling, sieving, panning, magnetic separation, and heavy liquid density separation using lithium metatungstate in the HSU mineral separation laboratory. After completing these steps for each individual sample, the separates were viewed under a high magnification light picking microscope. High quality grains of apatite or zircon; determined by properties including: euhedral structure, unbroken, lack of inclusions, staining, or pitting, were then picked from the separates and packed into niobium tubes. The packed grains were then shipped to the University of Colorado Thermochronology Research and Instrumentation Laboratory for (U-Th)/He analyses. Apatite grains from this study were analyzed using zircon degassing and isotope dilution methods to ensure grains containing small inclusions were dissolved completely. The grains were first degassed to extract and measure the radiogenic 4He with a quadrupole mass spectrometer. Then, the grains were dissolved in nitric or hydrofluoric acid and U, Th, and Sm ratios measured by an inductively coupled plasma

mass spectrometer. These element ratios were compared to produce a cooling age for each sample.

RESULTS

Apatite (U-Th)/He (AHe) and Zircon (U-Th)/He (ZHe) and ages were obtained from the Ashland, China Creek, Grayback, and Ironside Mountain plutons (Table 1) with the goal of determining timing of exhumation and constraining activity of associated Tertiary faults. Raw AHe and ZHe cooling age data including individual grain ages from bedrock samples are reported in Table 2 and Table 3.

Table 1. Bedrock sample location data from plutons analyzed for thermochronology.

Pluton	Sample Code	Latitude (°N)	Longitude (°W)	Elevation (m)
Ashland	AP01	42.0811	122.7050	2012
	AP03	42.0662	122.6703	1658
	AP06	42.1782	122.7189	711
	AP07	42.0767	122.6303	1475
China Creek	CH01	41.1056	123.0625	990
	CH02	41.0692	123.0788	1346
Grayback	GP01	42.1090	123.3028	1764
	GP02	42.1208	123.3100	2034
	GP03	42.1105	123.3060	1882
Ironside Mountain	DOIM17-04	40.8953	123.4667	1210

Table 2: Apatite (U-Th)/He data from the Klamath Mountain Province. r[a] represents equivelent spherical radius. T[b] indicates grain terminus; 0: Both tips broken. 1:One tip broken. 2: Whole grain. eU[c] - effective uranium concentration, weights U and Th for their alpha productivity, computed as [U] + 0.235 * [Th]. Ft[d] is alpha-ejection correction of Farley (2002). Analytical uncertainty based on U, Th, He, and grain length measurements. Grains less than 2.5ppm eU (in italics) not included in means.

Sample	Grain	Mass	r[a]	T[b]	He	U	Th	Sm	eU[c]	Th/U	Raw Date	Ft[d]	Date	2σ[e]
		(µg)	(µm)		(nmol/g)	(ppm)	(ppm)	(ppm)	(ppm)		(Ma)		(Ma)	(Ma)
AP06	a1	5.9	67.1	2	2.8	25.8	37.0	29.0	34.6	1.4	15	0.78	20	0.7
	a2	*0.9*	*34.0*	*2*	*0.0*	*0.0*	*2.0*	*0.4*	*0.5*	*63.0*	*0*	*0.54*	*1*	*24.2*
	a3	*0.9*	*N/A*	*2*	*0.0*	*0.1*	*0.0*	*1.6*	*0.1*	*0.0*	*N/A*	*N/A*	*N/A*	*N/A*
	a4	*1.2*	*N/A*	*2*	*0.0*	*0.0*	*0.0*	*1.8*	*0.0*	*N/A*	*N/A*	*N/A*	*N/A*	*N/A*
	a5	0.7	32.3	2	0.4	6.1	3.3	4.1	6.9	0.5	10	0.57	18	4.6
	a6	1.3	36.7	2	7.2	47.3	91.9	88.4	69.3	1.9	19	0.61	32	2.8
Mean age: 23.1± 7.7 Ma														
AP07	*a1*	*0.5*	*N/A*	*2*	*0.0*	*5.6*	*0.0*	*4.6*	*5.6*	*0.0*	*N/A*	*N/A*	*N/A*	*N/A*

Sample	Grain	Mass	r[a]	T[b]	He	U	Th	Sm	eU[c]	Th/U	Raw Date	Ft[d]	Date	2σ[e]
	a2	0.6	30.5	2	1.1	18.8	22.8	37.9	24.3	1.2	8	0.54	15	2.3
	a3	0.3	21.2	1	4.1	63.5	42.0	32.4	73.6	0.7	10	0.37	28	3.4
	a4	0.7	26.8	1	0.6	10.2	15.9	32.0	14.0	1.6	8	0.48	16	2.7
	a5	0.5	23.4	2	0.8	12.8	18.8	29.6	17.4	1.5	9	0.42	21	3.2
Mean age: 20.0 ± 5.7 Ma														
CH01	a1	2.5	48.0	2	2.7	11.3	28.3	122.6	18.2	2.5	28	0.69	40	3.6
	a2	*7.6*	*N/A*	*1*	*0.0*	*0.1*	*0.0*	*0.1*	*0.1*	*0.0*	*1*	*N/A*	*1*	*6.2*
	a3	4.7	62.8	1	2.4	11.9	27.9	86.8	18.7	2.3	24	0.76	32	1.3
	a4	4.7	61.8	2	3.9	13.4	33.5	102.2	21.5	2.5	33	0.76	44	2.0
	a5	3.1	54.4	2	3.0	11.5	26.0	97.4	17.8	2.3	31	0.73	42	2.6

Sample	Grain	Mass	r[a]	T[b]	He	U	Th	Sm	eU[c]	Th/U	Raw Date	Ft[d]	Date	2σ[e]
Mean age: 39.4 ± 2.4 Ma														
CH02	a1	5.3	64.9	2	4.9	41.5	48.6	67.8	53.2	1.2	17	0.78	22	1.1
	a3	3.4	57.1	2	5.4	52.4	62.1	94.3	67.3	1.2	15	0.75	20	0.6
	a4	5.6	67.4	2	4.5	30.3	37.1	55.6	39.2	1.2	21	0.78	27	0.9
	a5	2.4	50.8	2	5.2	46.2	58.3	98.4	60.2	1.3	16	0.71	22	1.2
Mean age: 22.8 ± 0.9 Ma														
GP02	a1	1.1	35.8	2	6.5	48.3	106.8	134.3	73.9	2.2	16	0.60	27	4.6
	a2	0.8	30.4	2	5.1	34.1	86.7	82.2	54.8	2.5	17	0.53	33	3.0
	a3	1.4	35.7	2	2.5	15.6	32.5	71.8	23.4	2.1	20	0.60	33	2.2
	a4	0.5	29.4	2	6.3	46.4	93.0	86.4	68.7	2.0	17	0.52	33	2.1

Sample	Grain	Mass	r[a]	T[b]	He	U	Th	Sm	eU[c]	Th/U	Raw Date	Ft[d]	Date	2σ[e]
	a5	1.1	38.4	2	0.1	1.9	3.1	3.3	2.7	1.6	10	0.63	16	7.5
Mean age: 28.3 ± 3.9 Ma														
DOIM17-04	a1	3.3	50.3	2	2.8	19.9	43.4	41.5	30.1	2.2	17	0.71	24	1.0
	a2	1.4	39.8	1	8.7	65.0	107.7	26.7	90.3	1.7	18	0.65	28	0.8
	a3	*0.4*	*25.6*	*2*	*12.7*	*73.9*	*127.0*	*29.7*	*103.7*	*1.7*	*23*	*0.45*	*50*	*1.9*
	a4	0.9	28.6	1	11.1	94.0	125.2	41.2	123.5	1.3	17	0.54	31	0.9
	a5	3.0	55.2	2	3.0	21.3	36.1	23.3	29.8	1.7	18	0.74	25	7.3
Mean age: 26.7 ± 3.1 Ma														

Table 3: Zircon (U-Th)/He data from the Klamath Mountain Province. r[a] represents equivelent spherical radius. T[b] indicates grain terminus; 0: Both tips broken. 1:One tip broken. 2: Whole grain. eU[c] - effective uranium concentration, weights U and Th for their alpha productivity, computed as [U] + 0.235 * [Th]. Ft[d] is alpha-ejection correction of Farley (2002). Analytical uncertainty based on U, Th, He, and grain length measurements. Grains less than 2.5ppm eU (in italics) not included in means.

Sample	Grain	Mass	r[a]	T[b]	He	U	Th	Sm	eU[c]	Th/U	Raw Date	Ft[d]	Date	2σ[e]
		(µg)	(µm)		(nmol/g)	(ppm)	(ppm)	(ppm)	(ppm)		(Ma)		(Ma)	(Ma)
AP01	z1	14.4	134.8	2	216.5	337.9	187.1	N/M	381.9	0.6	104	0.84	123	2.7
	z2	14.1	112.7	2	143.1	200.2	114.6	N/M	227.1	0.6	116	0.84	138	2.7
	z3	9.6	109.3	2	178.4	274.8	152.8	N/M	310.7	0.6	106	0.82	128	4.0
	z4	9.1	112.3	2	238.1	444.1	178.4	N/M	486.0	0.4	90	0.82	110	2.5

Sample	Grain	Mass	r[a]	T[b]	He	U	Th	Sm	eU[c]	Th/U	Raw Date	Ft[d]	Date	2σ[e]
	z5	13.7	117.0	2	219.3	381.4	160.7	N/M	419.2	0.4	96	0.84	114	3.0
Mean age: 122.6 ± 11.4 Ma														
AP06	z1	23.6	129.0	2	191.2	298.5	156.5	9.3	335.8	0.5	105	0.86	122	4.0
	z2	35.3	143.9	2	129.9	194.8	81.4	6.6	214.1	0.4	112	0.88	126	3.4
	z3	13.4	107.2	2	216.3	359.0	208.6	9.6	408.6	0.6	98	0.84	116	3.1
	z4	9.7	104.5	2	225.0	357.4	193.5	7.2	403.5	0.5	103	0.82	125	3.9

Sample	Grain	Mass	r[a]	T[b]	He	U	Th	Sm	eU[c]	Th/U	Raw Date	Ft[d]	Date	2σ[e]
	z5	4.9	63.4	2	237.8	400.7	203.2	7.0	449.1	0.5	98	0.77	127	3.7
Mean age: 123.3 ± 4.4 Ma														
GP02	z1	12.3	112.1	2	100.7	156.3	71.9	4.3	173.4	0.5	107	0.83	129	5.0
	z2	17.3	121.9	2	103.2	151.7	72.3	3.8	168.9	0.5	112	0.85	132	3.8
	z3	12.6	116.5	2	63.1	100.9	42.3	2.1	110.9	0.4	105	0.84	125	4.2
	z4	12.2	125.9	2	70.2	109.8	46.8	2.1	120.9	0.4	107	0.84	127	3.5

Sample	Grain	Mass	r[a]	T[b]	He	U	Th	Sm	eU[c]	Th/U	Raw Date	Ft[d]	Date	2σ[e]
	z5	6.8	92.2	2	77.1	126.7	49.8	3.3	138.5	0.4	102	0.80	129	4.5
Mean age: 128.2 ± 1.3 Ma														

Mean cooling age data are reported from north to south, where n=number of grain ages per sample. Bedrock sample GP02 from the Grayback pluton yielded a mean ZHe age of 128.2 ± 2.5 Ma (n=5) and mean AHe age of 28.3 ± 7.5 Ma (n=5). This sample was collected at 2034 m a.s.l. and is outside the known footprint of any Tertiary faults. The early Cretaceous ZHe age likely represents post-crystallization cooling after initial emplacement. The middle Oligocene AHe age is similar to other AHe ages found within the KMP.

Three bedrock samples from the Ashland pluton yielded two mean ZHe and two AHe ages, with one sample producing both an ZHe and AHe age. Sample AP01 yielded a mean ZHe age of 122.6 ± 11.4 Ma (n=5). Sample AP06 yielded a comparable mean ZHe age of 123.3 ± 4.4 Ma (n=5). Similarities between the AP01 and AP06 ZHe ages and the GP02 ZHe age show early Cretaceous regional cooling after crystallization and emplacement of the plutons, ca. 160-161 Ma. Sample AP06 yielded a mean AHe age of 23.1 ± 7.7 Ma (n=3) and sample AP07 yielded a mean AHe age of 20.0 ± 5.7 Ma (n=4). These samples, taken from the footwall of the SSF, record late Oligocene to early Miocene exhumation that postdates slip of the SSF, as SSF activity is geologically constrained to end by ~27 Ma (Figure 8). Sample AP07 was collected at an elevation 765 m above AP06. A younger AHe age at a higher elevation (AP07) is contrary to an expected, simplified cooling age-elevation relationship. This observation may be explained by the two ages being within uncertainty of each other or post emplacement rotation and tilting of the Ashland pluton potentially impacting its cooling history.

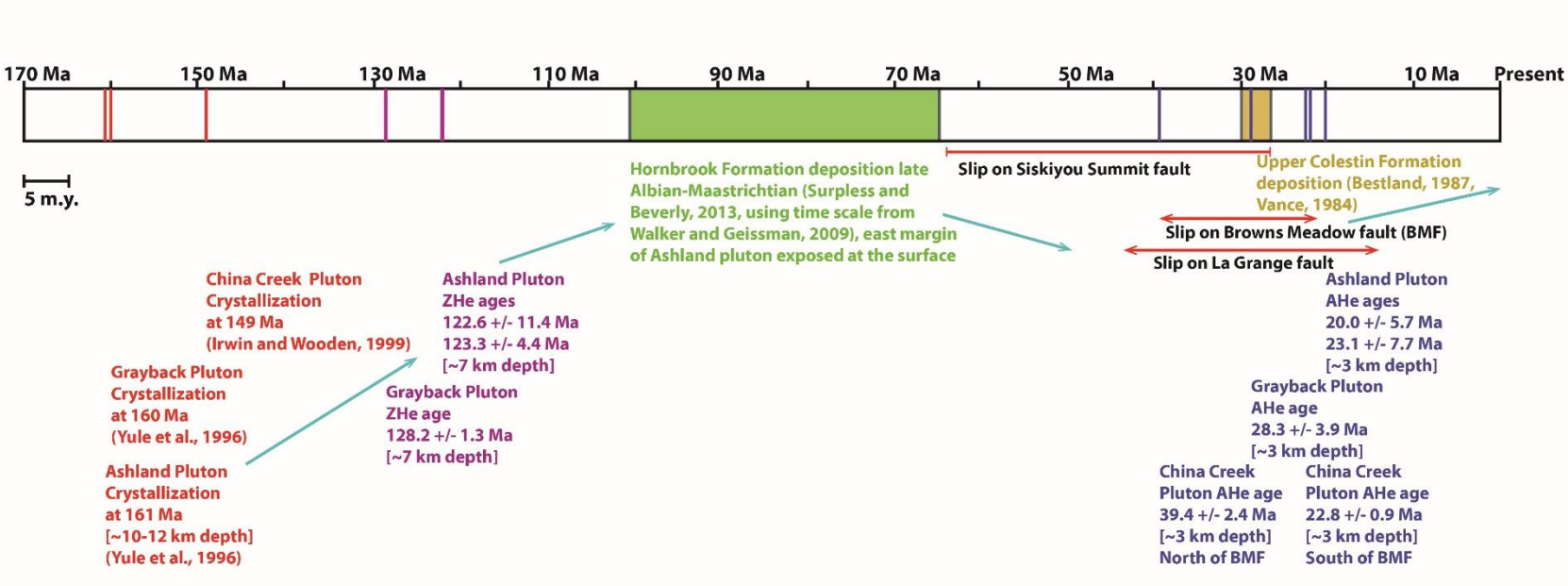

Figure 8. Timeline showing the annotated exhumation histories of the Grayback, Ashland, and China Creek plutons. Crystallization ages are shown in red, zircon (U-Th)/He cooling ages (ZHe) are shown in purple, apatite (U-Th)/He cooling ages (AHe) are shown in blue, and deposition of sedimentary units onlapping the Ashland pluton are shown in green and brown. The light-blue lines with arrows are representative of the exhumation path of the Ashland pluton to the surface.

Bedrock samples from the China Creek pluton produced two mean AHe ages from two samples collected on either side of the BMF. Sample CH01, from the downthrown block, yielded a mean AHe age of 39.4 ± 5.4 Ma (n=4). Sample CH02, from the upthrown block, yielded a mean AHe age of 22.8 ± 3.0 Ma (n=4). The two bedrock samples are ~4 km apart laterally and are separated by ~350 m of elevation (Figure 6).

Bedrock sample DOIM17-04 from the Ironside Mountain Batholith yielded a mean AHe age of 26.7 ± 3.1 Ma (n= 4). This sample was collected at 1210 m a.s.l. and is outside the known footprint of any Tertiary faults.

The AHe ages collected in this study are compiled with all existing, available AHe data (Batt et al., 2010a; Piotraschke et al., 2015; Team, 2018; Puleri et al., 2019; Pesek et al., 2020; Thompson Jobe et al., pers. comm., 2021) within and proximal to the KMP. Mean AHe ages are plotted separately against latitude and longitude of the samples in order to identify any relationships between AHe age and position relative to the CSZ (Figure 9). Mean AHe ages are also compared to elevation profiles to identify any potential cooling age-elevation relationships. AHe data are grouped into age brackets and plotted on a map with the Tertiary faults identified in this study to help further assess any spatial and temporal patterns of exhumation (Figure 10). The majority of AHe ages throughout the KMP are between 15-30 Ma, with the exception of a cluster of 30-40 Ma ages located in the south-central core of the KMP (Figure 10).

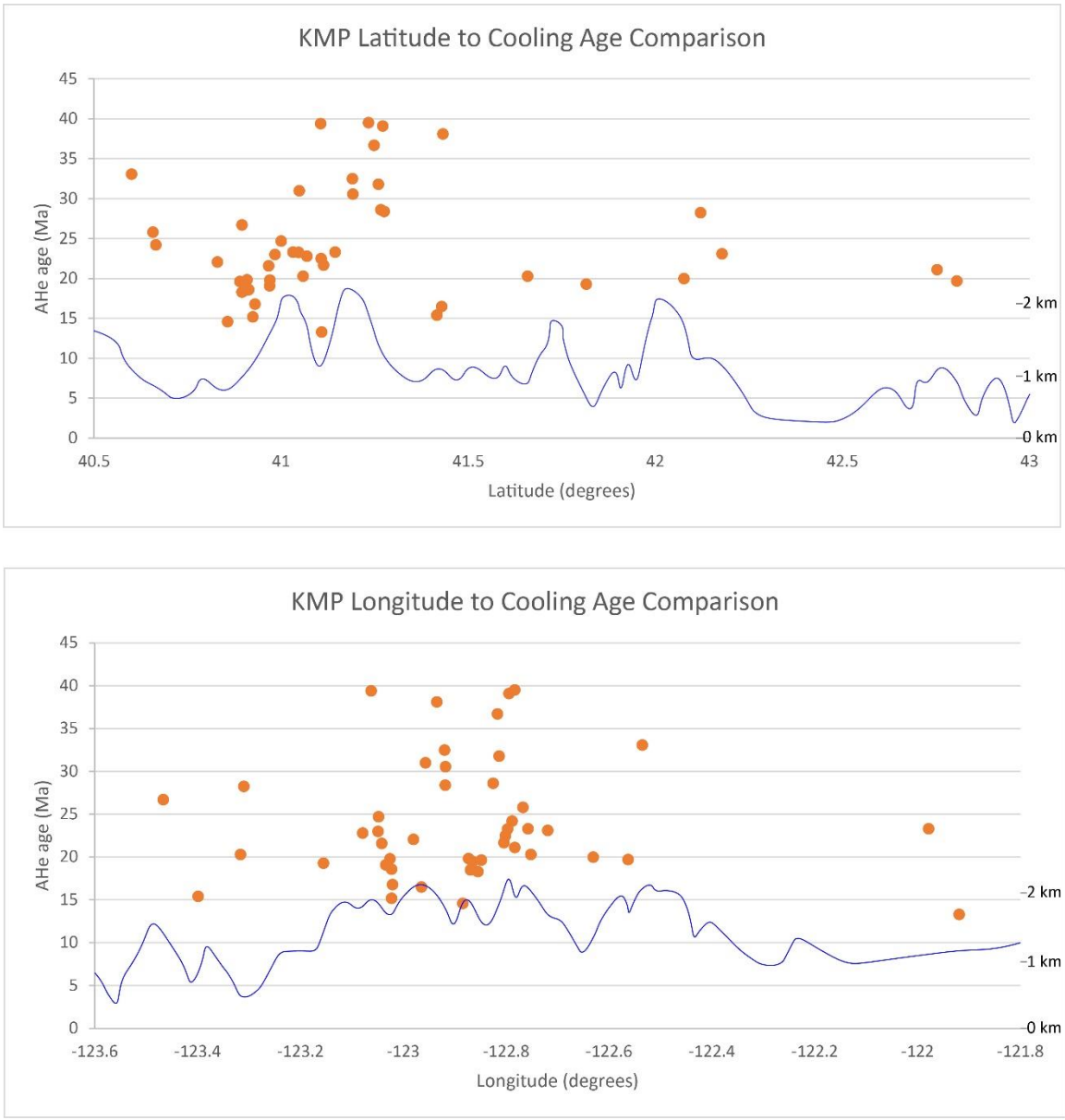

Figure 9. Top: Latitude of apatite (U-Th)/He cooling age (AHe) samples compared to the AHe age of the sample. Bottom: Longitude of AHe samples compared to the AHe age. For both, the blue line is a representative elevation profile of the KMP. AHe sample data for both graphs are compiled from this study, Batt et al. (2010a), Piotraschke et al. (2015), Team (2018), Puleri et al. (2019), Pesek et al. (2020), Thompson Jobe et al. (pers. comm., 2021).

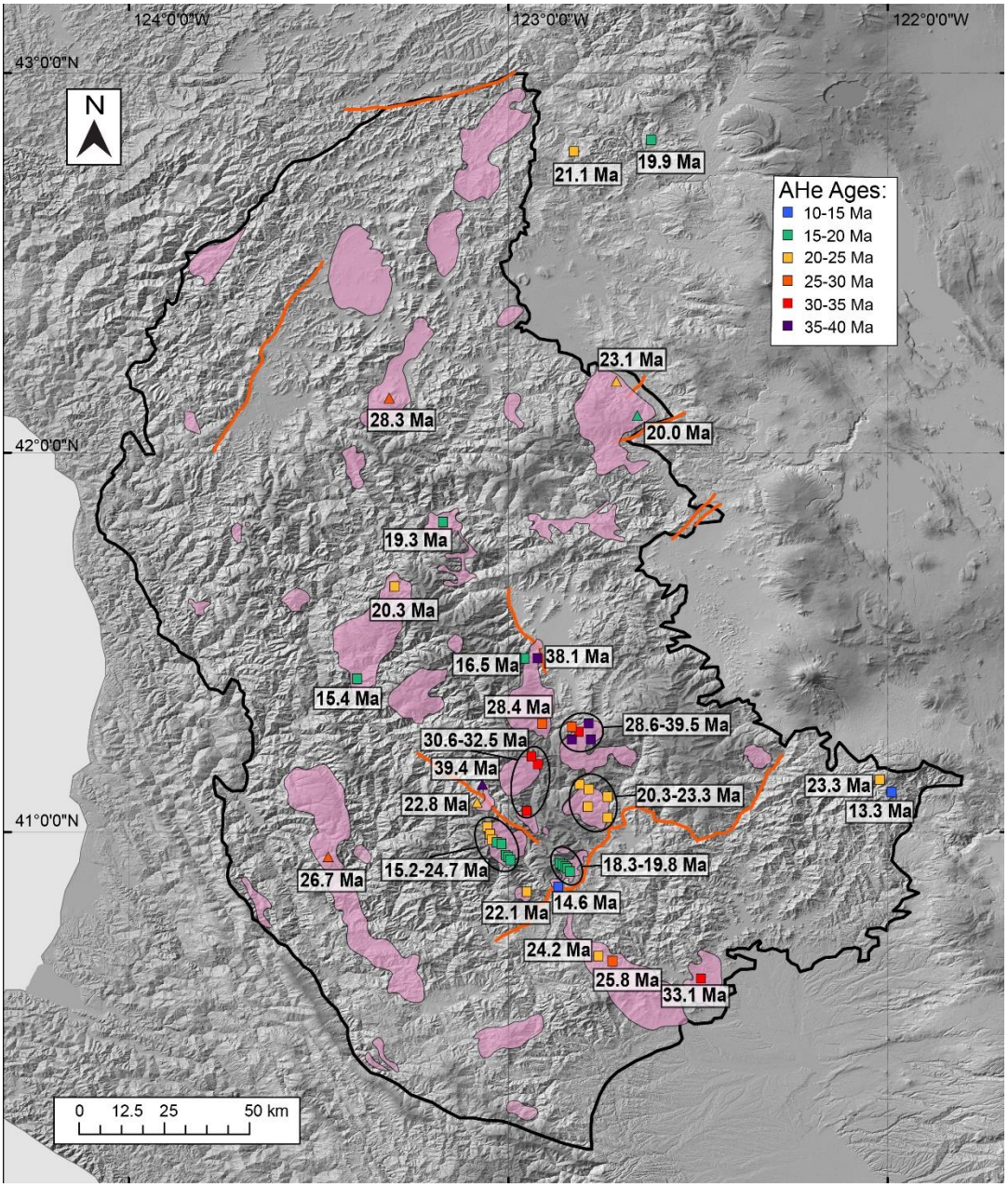

Figure 10. Map displaying all available apatite (U-Th)/He cooling age (AHe) data within and surrounding the Klamath Mountain Province (KMP). Samples are plotted by location, labeled with AHe age, and color coded by AHe age range. Samples tightly clustered within a specific geographic area are grouped together by black ovals and labeled with respective AHe age ranges. Samples from this study are denoted by a triangle symbol with all other samples denoted by a square symbol. AHe sample data are compiled from this study, (Batt et al., 2010a), (Piotraschke et al., 2015), (Team, 2018), (Puleri et al., 2019), (Pesek et al., 2020) (Thompson Jobe et al., pers. comm., 2021). Cenozoic faults (orange) and the KMP outline (black) were digitized from Irwin (1994). The hillshade background was constructed in ArcMap from 30 m SRTM DEM data.

Thermal Modeling

Time-temperature histories of samples from this study are obtained through inverse modeling of ZHe and AHe data using the HeFTy software package (Ketcham, 2005). HeFTy utilizes empirically obtained data, inputted time-temperature constraints, and measured (U-Th)/He data to model the diffusive behavior of radiogenic Helium in individual grains of apatite or zircon through time to produce time-temperature paths that are deemed good or acceptable (Ketcham, 2005).

Time-temperature histories from the northern KMP are obtained from ZHe and AHe data from samples AP06 and GP02 (Figure 11). Time-temperature constraints for sample AP06 include the ~161 Ma crystallization age of the Ashland pluton (Yule et al., 1996), onlapping deposition of the Hornbrook Formation on the eastern edge of the Ashland pluton exposed at the surface from late Albian to Maastrichtian time (Surpless and Beverly, 2013), and the exposure of the sample at the surface today. Time-temperature constraints for sample GP02 include the ~160 Ma crystallization age of the Grayback pluton (Yule et al., 1996), deposition of the nearby Sunset Road Quarry deposit (~30 km southwest of the Grayback pluton) from Coniacian to Campanian time (Surpless, 2015), and the exposure of the sample at the surface today. The best-fit models of samples AP06 and GP02 are similar, with rapid post-crystallization cooling up to ~100 Ma, followed by gradual cooling to ~35 Ma, followed by moderate to rapid cooling to the present (Figure 11).

Time-temperature histories from the south-central KMP are obtained from AHe data from samples CH01 and CH02 (Figure 12). Time-temperature constraints for samples CH01 and CH02 include the 149 Ma crystallization age of the China Creek pluton (Irwin and Wooden, 1999) and the exposure of the sample at the surface today. The best-fit model of CH01 records rapid cooling up until ~67 Ma, followed by gradual cooling to the present (Figure 12). The best-fit model of CH02 records semi-rapid cooling up to ~50 Ma, followed by gradual cooling through the 68 ± 5 ^{o}C AHe closure temperature (Farley, 2000) to ~18 Ma, followed by moderate cooling to the present (Figure 12).

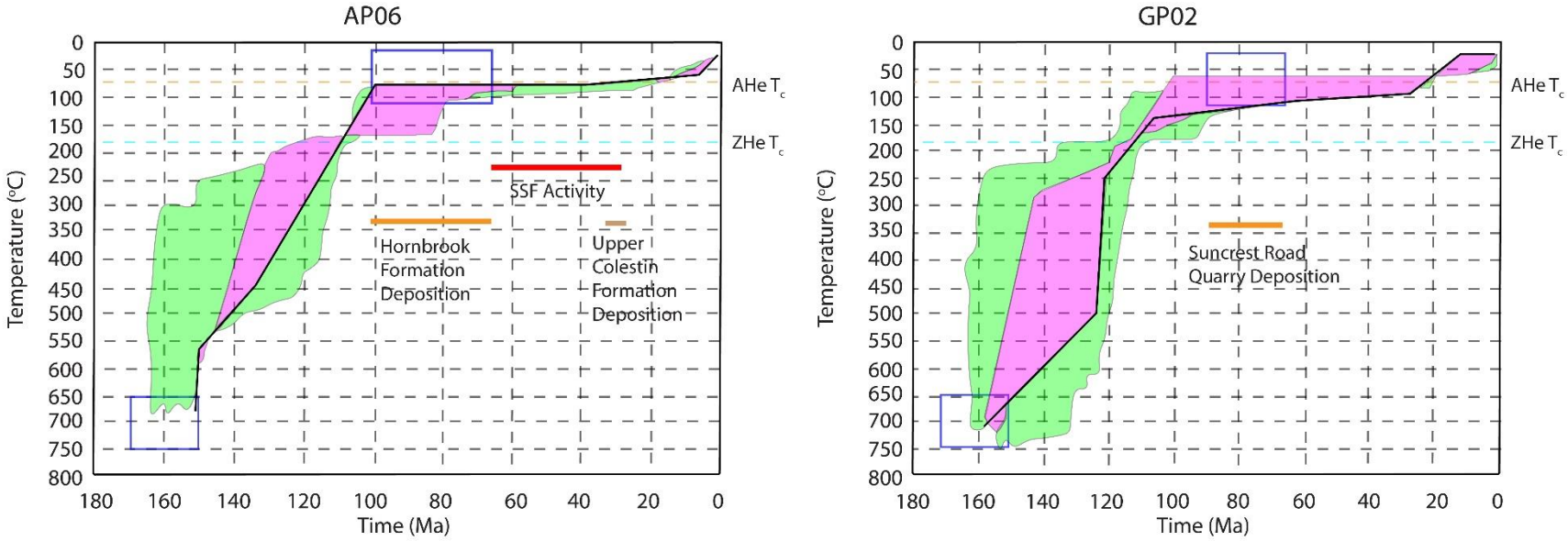

Figure 11. Time-temperature histories of samples AP06 (left) and GP02 (right) obtained from inverse modeling of zircon and apatite (U-Th)/He data using the HeFTy software package (Ketcham, 2005). Darker purple represents the good-fit path envelopes, lighter green represents the acceptable-fit path envelopes, and the solid black line shows the best-fit model. Blue boxes show inputted thermal constraint boxes from known crystallization ages of the Ashland and Grayback plutons (Barnes et al., 1995; Gribble et al., 1990; Yule et al., 1996), as well as known depositional ages of onlapping or proximal sedimentary deposits (Surpless and Beverly, 2013; Surpless, 2015) annotated by orange and brown timelines. Siskiyou Summit fault (SSF) activity is shown on the AP06 model by the red timeline. Apatite (U-Th)/He closure temperature (AHe T_c) is shown by the dashed orange line (Farley, 2000) and zircon (U-Th)/He closure temperature (ZHe T_c) is shown by the dashed teal line (Reiners et al., 2004).

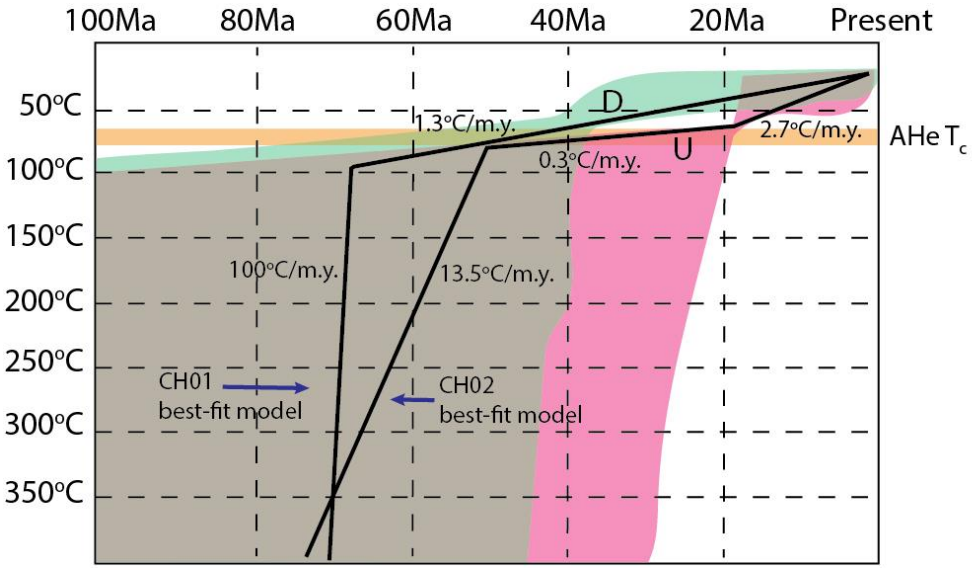

Figure 12. Combined time-temperature histories of samples CH01 and CH02 obtained from inverse modeling of apatite (U-Th)/He data using the HeFTy software package (Ketcham, 2005). Lighter green (running from roughly 100 °C to 25 °C in the upper portion of the figure) represents the good-fit path envelope of sample CH01 from the downthrown block (D) of the Browns Meadow fault (BMF), darker pink (starting at roughly 40 Ma on the right side of the figure) represents the good-fit path envelope of sample CH02 from the upthrown block (U) of the BMF, and medium gray (located in between the lighter green and darker pink areas, starting at 100 Ma) represents overlap of the good-fit path envelopes. The solid black lines show the best-fit model of each sample, labeled by the blue arrows. Estimated cooling rates for individual segments of each best-fit model are labeled. Apatite (U-Th)/He closure temperature (AHe T_c) with uncertainty is labeled and shown by the horizontal shaded orange line (Farley, 2000).

DISCUSSION

By analyzing the geometry and slip on two poorly constrained Tertiary faults in the KMP, i.e., SSF and BMF, and using thermochronology to constrain the timing of exhumation of footwall rocks, I show how Tertiary faults outside of the LGF significantly impacted exhumation in both the southern and northern KMP. Previous studies of Tertiary faulting in the KMP were regionally restricted and focused on the LGF, using thermochronology to constrain timing and slip. In this study, I first analyze data compiled from geologic maps and cross sections, in addition to thermochronology, to constrain the activity and style of faulting for the BMF and SSF. Then, I compile all thermochronologic data in the KMP to determine any spatial or temporal patterns in rock cooling and exhumation. Finally, I evaluate apparent cooling patterns in context of potential mechanisms driving regional or local exhumation.

Siskiyou Summit Fault

The SSF is a normal fault with a surface trace of >24 km located in the northeastern KMP, with activity geologically constrained to ~65-27 Ma, offsetting the Jurassic Ashland pluton and Cretaceous to Tertiary sedimentary units (Wells, 1956; Vance, 1984; Bestland, 1987). A horizontal separation of 11.3 km of the contact between the Hornbrook Formation and overlying Umpqua Formation, along with Hornbrook Formation bedding attitudes ranging from 25^{o}-30^{o} (Wells, 1956), are used with trigonometry to estimate a vertical offset ranging between 5.3-6.5 km (Figure 5).

Assuming the SSF was active throughout the time period constrained by the onlapping geologic units and that erosion was not a factor, a minimum exhumation rate of 0.16 km/m.y. is required to yield the apparent ~6 km vertical offset. Considering sedimentological evidence the SSF was primarily active during younger section of the ~65-27 Ma bracketed time window (Bestland, 1987), a exhumation rate of 0.46 km/m.y. between ~40-27 Ma is required to yield the apparent ~6 km vertical offset. Low temperature thermochronology is used on bedrock samples from locations of the Ashland pluton located in the footwall of the SSF to evaluate whether SSF activity is recorded in the pluton's cooling signal.

Cooling ages from the Ashland pluton fall outside of the geologically constrained activity of the SSF. ZHe ages record post emplacement cooling prior to SSF activity (123.3 Ma, 122.6 Ma ZHe ages), as well as continued cooling shortly after SSF activity ceased (23.1 Ma, 20.0 Ma AHe ages). The lack of cooling ages within the geologically constrained SSF activity does not rule out the role of the SSF in exhuming the Ashland pluton, but shows how additional mechanisms other than SSF-driven exhumation must have contributed to exhumation. This new thermochronologic data and investigation into the SSF provides a more complete exhumation history of the Ashland pluton. After crystallization at ~161 Ma, ZHe ages of 122.6 and 123.3 Ma record post emplacement cooling, followed by exhumation to the surface suggested by onlapping deposition of the late Cretaceous Hornbrook formation (Figure 8). Deposition of the Hornbrook formation also marks partial reburial of the Ashland pluton to at least ~5 km depth, evident by proximal reset AHe ages (Batt et al., 2010b), preceding fault-driven exhumation of the

SSF from ~40-27 Ma, followed by continued exhumation to the near surface recorded by early Miocene AHe ages, 20.0 and 23.1 Ma (Figure 8).

Eastward dip observations of the Hornbrook formation onlapping the Ashland pluton indicates the Ashland pluton experienced a minimum of 25^{o} tilt towards the ENE since the Cretaceous (Wells, 1956; Barnes et al., 1986b). To the southwest of the Ashland pluton and Condrey Mountain area lies the Wooley Creek batholith. Observations of exposed contact metamorphic assemblages indicate the Wooley Creek batholith experienced a minimum of 30^{o} tilt towards the WSW (Barnes et al., 1986b). Mortimer and Coleman (1985) proposed the observation of tilted plutons and strata in the KMP could be explained by a Neogene aged regional structural dome composed of the Condrey Mountain terrane (Figure 2B). Mid Eocene to late Oligocene apatite fission track ages from the Wooley Creek batholith and Slinkard pluton, located closest to the center of the Condrey Mountain area, indicate primary rock uplift occurred prior to the Neogene (Piotraschke et al., 2015). AHe ages from the Slinkard pluton (19.3 Ma) and northern end of the Wooley Creek batholith (20.3 Ma) (Piotraschke et al., 2015) are similar to those observed in the Ashland pluton, indicating the plutons were at a similar crustal level, ~2.5 km, during this time. However, a sample from the southern, tilted end of the Wooley Creek batholith records a younger AHe age of 15.4 Ma (Piotraschke et al., 2015). Although the mean AHe ages between AP06 and AP07 are within uncertainty of one another, the observation of an older cooling age at a lower elevation in the Ashland pluton may be explained by the tilting of the pluton. However, samples AP06 and AP07 are both located on the northeast edge of the pluton, and are not separated in the direction

of tilt (Figure 4). Therefore, it is unlikely that tilting can explain the discrepancy between the AHe ages. On the other hand, similarities between the Ashland AHe ages and AHe ages from Wooley Creek and Slinkard potentially support a broad, regional exhumation signal in the northern KMP, potentially driven by structural doming in the Condrey Mountain area, prior to the previously suggested Neogene window.

The observation of broad, regional exhumation in the northern KMP is further supported by similarities between ZHe and AHe ages from the Ashland and Grayback pluton (separated by ~50 km), in addition to time-temperature histories obtained from thermal modeling (Figure 11). After crystallization of the Grayback pluton at ~160 Ma, a 128.2 Ma ZHe age records post emplacement cooling, followed by continued exhumation through the upper crust recorded by a 28.3 Ma AHe age. Similarities between the thermal histories of the Ashland and Grayback plutons show how crustal exhumation in the northern KMP may have occurred at a regional level in Tertiary time. These similarities suggest both plutons underwent similar exhumation histories, albeit, the Ashland pluton's history was potentially more complex due to SSF activity and observed tilting of the pluton and strata in the area.

Browns Meadow Fault

The BMF is a high angle fault containing the high relief Trinity Alps area within its upthrown block to the south. The high angle geometry of the fault and challenging terrain and Mesozoic geology of the area make it difficult to determine whether the BMF

displays normal or reverse motion. However, cooling age data and general observations of topography both support tectonic uplift in the southern, upthrown block of the BMF.

The close spatial proximity and cooling age difference between CH01 (39.4 Ma AHe age) and CH02 (22.8 Ma AHe age) provide evidence the BMF was at least partially responsible for exhumation of plutons located in the fault's upthrown block (Figure 6). Assuming a 68^{o} C apatite He closure temperature, 10^{o} C surface temperature, and 20^{o} C/km geothermal gradient, the differential in cooling rates from each sample require a minimum of ~1 km of vertical offset by the BMF. This estimation is supported by a geologic cross section across the BMF that shows similar apparent vertical offset of the Siskiyou Thrust fault (Figure 7). The disparity between AHe ages from CH01 and CH02, as well as AHe data from proximal plutons on either side of the fault (Figure 6), provide clear evidence rock cooling in the south-central KMP was significantly affected by the BMF, in addition to the LGF. Time-temperature histories obtained from thermal modeling of samples CH01 and CH02, show how cooling in the downthrown block was relatively gradual during Tertiary time, compared to cooling in the upthrown block (Figure 12). The best-fit model of sample CH02 also suggests more rapid cooling in the upthrown block of the BMF initiated by ~18 Ma (Figure 12), potentially indicating when BMF activity initiated or when activity was at its peak. The modeling is not able to predict the duration or cessation of slip.

The Neogene southward progression of detachment-driven exhumation of the LGF may have been coeval with slip on the BMF, leading to accelerated exhumation and younger AHe ages to the south. Exhumation in the south-central KMP is complicated by

this new understanding that both the LGF and BMF influenced cooling ages. The regional cluster of 30-40 Ma AHe ages located in the south-central KMP (Figure 10) is bound by the BMF to the southwest and LGF to the southeast. Piotraschke et al. (2015) argued the older AHe ages represent the core of the LGF footwall, and that younger AHe ages to the south represent the most recent exhumation of the LGF as hanging wall rocks were transported southward during detachment. Although AFT data are more sparse in the KMP, AFT ages are consistent with this pattern with the oldest ages, ~75-95 Ma, found in the south-central core (Batt et al., 2010a). These new data show the BMF may have accelerated exhumation of plutons located in the upthrown block of the BMF to the south, i.e., Canyon Creek, Granite Peak, potentially halting LGF exhumation of plutons in the downthrown block, i.e., Deadman Peak (Figure 7). Slip on the LGF was previously constrained to a rate of 2 km/m.y. between 45 to 15 Ma (Cashman and Cashman, 2006; Piotraschke et al., 2015). This unusually low slip rate suggests the LGF either had relatively slow activity over time, or the assumed time the LGF was active may be inaccurate. With an apparent vertical offset of ~1-1.5 km for the BMF, an assumed slip rate is required to determine how long the BMF was potentially active. However, previous studies (Team, 2018) have constrained an exhumation rate for the Canyon Creek pluton, located in the upthrown block of the BMF. Similarities between the Canyon Creek pluton AHe ages and the 22.8 Ma AHe age from CH02 (Figure 6), indicate the Canyon Creek pluton and the section of the China Creek pluton located in the upthrown block of the BMF were exhumed at a similar time. AHe ages from the Canyon Creek pluton record an exhumation rate of 0.14 km/m.y. from 24.7-15.2 Ma (Team, 2018).

Assuming this exhumation rate may record slip of the BMF and could act as a first-order estimation for vertical slip rate, with zero erosion the BMF would have to have been active for a maximum of ~7 m.y. to produce the observed ~1-1.5 km of apparent vertical offset.

Finally, these new data also show the trace of the previously mapped BMF may be misrepresented. The 31.4 Ma AHe age from the Caribou Mountain pluton (Piotraschke et al., 2015) falls more within the pattern of AHe ages north of the BMF, versus the younger AHe ages south of the BMF, indicating the BMF trace may continue southeast versus veering directly east at the Caribou Mountain pluton (Figure 6). There must still be a fault where the BMF is mapped with an eastern trace, but it may be an older structure. The linear fault trace of the BMF indicates the BMF has a high angle, making it more kinematically complicated for the fault to change directions in trace, further supporting this new interpretation. The results from this study and geometry of the fault both indicate the BMF fault trace continues southeast separating the Caribou Mountain and Canyon Creek plutons (Figure 10).

Regional Exhumation Patterns

To address patterns in cooling age spatial distribution, the location of AHe samples are compared to their age and an elevation profile parallel to the latitude or longitude of the samples (Figure 9). The lack of correlation between AHe age and elevation shows crustal exhumation was not temporally uniform throughout the entire KMP during Tertiary time, which is not unexpected given the knowledge of location and

timing of LGF-driven exhumation (Figure 9). The lack of correlation between AHe age and latitude shows change in position along strike of the CSZ did not influence Tertiary exhumation in the KMP (Figure 9). Finally, the lack of correlation between AHe age and longitude indicates how distance from the CSZ trench also did not influence Tertiary exhumation in the KMP (Figure 9). These observations indicate subduction zone dynamics were not the primary control on Tertiary exhumation. Tertiary exhumation was influenced both by Tertiary faulting and an early-mid Miocene widespread regional uplift and erosion event that appears to have affected the southern and northern KMP.

These new data, combined with known geologic constraints and previous thermochronologic studies, show the LGF, BMF, and SSF were potentially all active during the late Eocene to early Oligocene (Figure 8). If the faults were synchronously active, this indicates Tertiary tectonic activity in the KMP was at a peak during this time period. The position of the cluster of older AHe ages relative to the BMF and LGF indicate Tertiary faulting significantly influenced exhumation in the south-central KMP. Plutons within the upthrown block of the BMF and the footwall of the LGF, i.e., Canyon Creek and Granite Peak, contain some of the youngest AHe ages (15-20 Ma), indicating where the most recent tectonically-driven exhumation in the KMP occurred.

Margin-parallel extension is observed in the forearc to the north of the KMP during this time period, evident by regional dike swarms of the Tillamook magmatic episode, ca. 42-34 Ma (Wells et al., 2014). Wells et al. (2014) hypothesized interactions between the North American plate and the Yellowstone Hotspot (YHS) produced the Tillamook magmatic episode and associated margin-parallel extension. Piotraschke et al.

(2015) acknowledged the potential for YHS interactions also prompting extension and unroofing of the KMP via the LGF detachment system, but favored the idea of extension initiated by reorganization of the subduction zone following accretion of the Siletz terrane, ca. 51-49 Ma (Wells et al., 2014). Data from this study do not favor either mechanism initiating extensional tectonics, but show Tertiary tectonic activity was more pervasive throughout the KMP than previously thought, most evident by SSF activity in the northern KMP accompanying activity of the BMF and LGF in the southern KMP.

If one ignores the cluster of older AHe ages in the south-central core of the KMP, or assumes the south-central core area continued to exhume after cooling was recorded by low-temperature thermochronology, it becomes evident that exhumation throughout the KMP was relatively uniform, with the majority of AHe ages falling into the 20-25 Ma range, even in the absence of localized, known structures (Figure 10). The plutons sampled in this study located outside of the LGF footprint and any other known fault, i.e., Grayback and Ironside Mountain, produced AHe ages that also fit within this range. The Grayback pluton is the farthest northwest pluton sampled for thermochronology in the KMP and Ironside Mountain is the farthest southwest pluton sampled. The 28.3 Ma AHe age from Grayback and the 26.7 Ma AHe age from Ironside show relatively uniform exhumation of the western KMP in the middle Oligocene. As a whole, the late Oligocene to early Miocene cooling signal shows the time period where the majority of KMP rocks were being exhumed from ~2.5 km depth to the surface, perhaps generating the modern topography. Without any known distinct tectonic or climatic events occurring in this time period near the KMP, and no clear pattern relative to position of the CSZ, it is difficult to

tie the timing of this regional cooling signal to a specific mechanism. This cooling signal is older than cooling ages recorded in the forearc to the north in Oregon and Washington, indicating the most recent exhumation in the KMP appears to have occurred prior to the rest of the CSZ forearc.

CONCLUSIONS

Tertiary faulting activity within the Klamath Mountains Province (KMP) was more pervasive than previously thought, evident by constrained fault activity of the Siskiyou Summit fault (SSF) in the northeast KMP, and the Browns Meadow fault (BMF) and La Grange fault (LGF) in the south-central KMP. On the contrary, there are few mapped Quaternary faults within the province. This observation may be a product of the lack of Quaternary units in the KMP possibly related to disturbances of the landscape by hydraulic mining in the 19-20th century. An alternate possibility is a lack of tectonic activity in Quaternary time, with the exception of seismicity observed in the down-going plate beneath the KMP (Bostock et al., 2019). In this study, I identify all major Tertiary faults within the KMP. From these faults, I focus on three of the largest, the LGF, BMF, and SSF.

I use low temperature thermochronology to determine the timing of crustal exhumation from the northern to south-central KMP, and focus on determining the cooling rates and timing within and outside of the footprints of the major faults described above. The spatial distribution of (U-Th)/He cooling ages within the KMP indicate when and where crustal exhumation was occurring. The majority of AHe cooling ages are temporally clustered between 15-30 Ma and cover a large geographic footprint, with the notable exception of a grouping of older 30-40 Ma AHe ages located in the south-central core of the KMP. The older AHe ages in this area have been interpreted to be a result of LGF detachment driven exhumation occurring with a southward progression of slip that

was inferred to have initiated ~45 Ma (Piotraschke et al., 2015). These older cooling age data come from plutons located in the northern extent of the footwall and thus were exhumed first during initial LGF activity.

The BMF is a distinctive Tertiary fault in the KMP as it strikes northwest, is steeply dipping, and displays relative motions of footwall up to the south and hanging wall down to the north, opposite of the nearby LGF. AHe ages from the China Creek pluton, displaced by the BMF, provide insight into the apparent boundary between the older and younger AHe data. The cooling age differential allows for an estimation of vertical separation produced by fault slip, and bracket timing of fault activity. A 39.0 Ma AHe age from the downthrown block and 22.8 Ma AHe age from the upthrown block, laterally separated by 4.4 km, likely record crustal cooling related to BMF activity. First, these data and thermal models constrain BMF fault activity to early Miocene at a maximum, and possibly younger. Second, the pattern of cooling ages proximal to the BMF indicate that it played a more important role in regional Tertiary exhumation than previously recognized, as the BMF and LGF are found to potentially be coeval, requiring another assessment of cooling ages previously attributed to detachment-driven exhumation of the LGF.

Geologic constraints suggest the SSF was active between ~65-27 Ma, most likely between 40-27 Ma, based on stratigraphic relations. By assigning known geometry of the fault, measuring apparent horizontal offset of displaced Tertiary units onlapping the Ashland pluton, and using measured bedding attitudes of the Hornbrook Formation, it is likely the Ashland pluton was exhumed vertically 5.3-6.5 km in the footwall of the SSF.

AHe ages of 19.9 Ma and 23.1 Ma from the Ashland pluton record exhumation that postdates slip of the SSF. A 28.3 Ma AHe age from the nearby Grayback pluton, combined with the Ashland AHe data, record a regional exhumation signal in the Northern KMP during the late Oligocene to early Miocene that cannot be attributed to fault-driven exhumation solely because the Grayback pluton appears to be unaffected by Tertiary-aged faulting.

This late Oligocene to early Miocene regional exhumation signal extends from the northern KMP to throughout most of the province with the notable exception of the south-central core. These AHe data capture exhumation driven by localized faulting of the LGF and BMF, but also regional exhumation driven by a mechanism that does not correlate temporally to previously identified mechanisms such as the collision of Siletzia or migration of the Mendocino Triple Junction. A lack of correlation between latitude or longitude and AHe ages in the KMP shows distance from the trench and position along strike of Cascadia does not appear to be linked to spatial patterns of Tertiary exhumation. With the lack of correlation between AHe age and position relative to the trench, it is possible the regional exhumation signal of the KMP is driven by regional erosion related to climatic factors or widespread uplift.

REFERENCES

Aalto, K.R., 2006, The Klamath peneplain: A review of J.S. Diller's classic erosion surface. Geological Society of America Special Paper 410, p. 451–464, doi: 10.1130/2006.2410(11).

Allen, C.M. and Barnes, C.G., 2006, Ages and some cryptic sources of Mesozoic plutonic rocks in the Klamath Mountains, California and Oregon: Geological Society of America Special Paper 410, p. 223–245, doi: 10.1130/2006.2410(11).

Barnes, C.G., Allen, C.M. and Saleeby, J.B., 1986a, Open-and closed-system characteristics of a tilted plutonic system, Klamath Mountains, California: Journal of Geophysical Research, v. 91, p. 6073-6090, https://doi.org/10.1029/JB091iB06p06073

Barnes, C.G., Rice, J.M. and Gribble, R.F., 1986b, Tilted plutons in the Klamath Mountains of California and Oregon: Journal of Geophysical Research: Solid Earth, v. 91, p. 6059-6071, https://doi.org/10.1029/JB091iB06p06059

Barnes, C.G., Petersen, S.W., Kistler, R.W., Prestvik, T., and Sundvoll, B., 1992, Tectonic implications of isotopic variation among Jurassic and Early Cretaceous plutons, Klamath Mountains: Geological Society of America Bulletin, v. 104, p. 117-126, https://doi.org/10.1130/0016-7606(1992)104<0117:TIOIVA>2.3.CO;2

Barnes, C.G., Johnson, K., Barnes, M.A., Prestvik, T., Kistler, R.W., and Sundvoll, B., 1995, The Grayback pluton: magmatism in a Jurassic back-arc environment, Klamath Mountains, Oregon: Journal of Petrology, v. 36, p. 397-415, https://doi.org/10.1093/petrology/36.2.397

Batt, G.E., Cashman, S.M., Garver, J.I. and Bigelow, J.J., 2010a, Thermotectonic evidence for two-stage extension on the Trinity detachment surface, Eastern Klamath mountains, California: American Journal of Science, v. 310, p. 261-281, doi: 10.2475/04.2010.02.

Batt, G.E., Harper, G.D., Heizler, M., and Roden-Tice, M., 2010b, Cretaceous sedimentary blanketing and tectonic rejuvenation in the Western Klamath mountains: Insights from thermochronology: Central European Journal of Geosciences, v. 2, p. 138-151, https://doi.org/10.2478/v10085-009-0041-4

Bestland, E.A., 1987, Volcanic stratigraphy of the Oligocene Colestin Formation in the Siskiyou Pass area of southern Oregon: Oregon Geology, v. 49, p. 79-86.

Blakely, R.J., Christiansen, R.L., Guffanti, M., Wells, R.E., Donnelly-Nolan, J.M., Muffler, L.P., Clynne, M.A. and Smith, J.G., 1997, Gravity anomalies, Quaternary vents, and Quaternary faults in the southern Cascade Range, Oregon and California: Implications for arc and backarc evolution: Journal of Geophysical Research: Solid Earth, v. 102, p. 22513-22527, https://doi.org/10.1029/97JB01516

Bostock, M.G., Christensen, N.I. and Peacock, S.M., 2019, Seismicity in Cascadia: Lithos, v. 332, p. 55-66, https://doi.org/10.1016/j.lithos.2019.02.019

Cashman, S.M. and Elder, D.R., 2002, Post-Nevadan detachment faulting in the Klamath Mountains, California: Geological Society of America Bulletin, v. 114, p. 1520-1534, https://doi.org/10.1130/0016-7606(2002)114<1520:PNDFIT>2.0.CO;2

Cashman, S.M. and Cashman, K.V., 2006 Cataclastic textures in La Grange fault rocks, Klamath Mountains, California: Geological Society of America Special Paper 410, p. 433-450, doi: 10.1130/2006.2410(11).

Cotkin, S.J. and Medaris Jr, L.G., 1993, Evaluation of the crystallization conditions for the calcalkaline Russian Peak intrusive complex, Klamath Mountains, northern California: Journal of Petrology, v. 34, p. 543-571, https://doi.org/10.1093/petrology/34.3.543

Davis, G.A., 1968, Westward thrust faulting in the south-central Klamath Mountains, California: Geological Society of America Bulletin, v. 79, p. 911-934, https://doi.org/10.1130/0016-7606(1968)79[911:WTFITS]2.0.CO;2

Diller, J.S., 1902, Topographic development of the Klamath Mountains: U.S. Geological Survey Bulletin 196, 69 p.

Enkelmann, E., Ehlers, T.A., Merli, G. and Methner, K., 2015, Thermal and exhumation history of the Eocene Chumstick Basin, Washington State, USA: Tectonics, v. 34, p. 951-969, https://doi.org/10.1002/2014TC003767

Farley, K.A., 2000, Helium diffusion from apatite: General behavior as illustrated by Durango fluorapatite: Journal of Geophysical Research: Solid Earth, v. 105, p. 2903-2914, https://doi.org/10.1029/1999JB900348

Farley, K.A., 2002, (U-Th)/He dating: Techniques, calibrations, and applications: Reviews in Mineralogy and Geochemistry, v. 47, p. 819-844, https://doi.org/10.2138/rmg.2002.47.18

Foster, D.A. and John, B.E., 1999, Quantifying tectonic exhumation in an extensional orogen with thermochronology: examples from the southern Basin and Range

Province: Geological Society, London, Special Publications, v. 154, p. 343-364, https://doi.org/10.1144/GSL.SP.1999.154.01.16

Gribble, R.F., Barnes, C.G., Donato, M.M., Hoover, J.D., Kistler, R.W., 1990, Geochemistry and Intrusive History of the Ashland Pluton, Klamath Mountains, California and Oregon: Journal of Petrology, v. 31, p. 883-923, https://doi.org/10.1093/petrology/31.4.883

Harper, G.D., Saleeby, J.B. and Heizler, M., 1994, Formation and emplacement of the Josephine ophiolite and the Nevadan orogeny in the Klamath Mountains, California-Oregon: U/Pb zircon and 40Ar/39Ar geochronology: Journal of Geophysical Research, v.99, p.4293-4321, https://doi.org/10.1029/93JB02061

Holm, D.K., Snow, J.K. and Lux, D.R., 1992, Thermal and barometric constraints on the intrusive and unroofing history of the Black Mountains: Implications for timing, initial dip, and kinematics of detachment faulting in the Death Valley region, California: Tectonics, v. 11, p. 507-522, https://doi.org/10.1029/92TC00211

Irwin, W.P., 1960, Geologic reconnaissance of the northern Coast Ranges and Klamath Mountains, California, with a summary of the mineral resources: California Division of Mines Bulletin, v. 179, p. 1-80.

Irwin, W.P., 1966, Geology of the Klamath Mountains province: California Division of Mines and Geology Bulletin, v. 190, p. 19-38.

Irwin, W.P., 1972, Terranes of the Western Paleozoic and Triassic Belt in the Southern Klamath Mountains, California: U.S. Geological Survey Professional Paper 800-C, p. C103–C111.

Irwin, W.P., 1985, Age and tectonics of plutonic belts in accreted terranes of the Klamath Mountains, California and Oregon, *in* Howell, D.G., ed., Tectonostratigraphic Terranes of the Circum-Pacific Region: Circum-Pacific Council for Energy and Mineral Resources Earth Science Series 1, p. 187–199.

Irwin, W.P., 1994, Geologic Map of the Klamath Mountains, California and Oregon: US Geological Survey, No. 2148, scale 1:500,000, doi: 10.3133/i2148

Irwin, W. P. and Wooden, J. L., 1999, Plutons and Accretionary Episodes of the Klamath Mountains, California and Oregon: U. S. Geological Survey Open-File Report 99-374, https://pubs.usgs.gov/of/1999/0374/.

Irwin, William P., 2003, Correlation of the Klamath Mountains and Sierra Nevada: U. S. Geological Survey Open-File Report 02-490, https://pubs.usgs.gov/of/2002/0490/.

Kelsey, H.M., Engebretson, D.C., Mitchell, C.E. and Ticknor, R.L., 1994, Topographic form of the Coast Ranges of the Cascadia margin in relation to coastal uplift rates and plate subduction: Journal of Geophysical Research: Solid Earth, v. 99, p. 12245-12255, https://doi.org/10.1029/93JB03236

Ketcham, R.A., 2005, Forward and inverse modeling of low-temperature thermochronometry data: Reviews in Mineralogy and Geochemistry, v. 58, p. 275-314, https://doi.org/10.2138/rmg.2005.58.11

Magill, J. and Cox, A., 1981, Post-Oligocene tectonic rotation of the Oregon western Cascade Range and the Klamath Mountains: Geology, v. 9, p. 127-131, https://doi.org/10.1130/0091-7613(1981)9<127:PTROTO>2.0.CO;2

Magill, J.R., Wells, R.E., Simpson, R.W. and Cox, A.V., 1982, Post 12 my rotation of southwest Washington: Journal of Geophysical Research: Solid Earth, v. 87, p. 3761-3776, https://doi.org/10.1029/JB087iB05p03761

Mankinen, E.A. and Irwin, W.P., 1982, Paleomagnetic study of some Cretaceous and Tertiary sedimentary rocks of the Klamath Mountains province, California: Geology, v. 10, p. 82-87, https://doi.org/10.1130/0091-7613(1982)10<82:PSOSCA>2.0.CO;2

Mankinen, E.A., Irwin, W.P., and Grommé, C.S., 1989, Paleomagnetic study of the Eastern Klamath terrane, California, and implications for the tectonic history of the Klamath Mountains province: Journal of Geophysical Research: Solid Earth, v. 94, p. 10444-10472, https://doi.org/10.1029/JB094iB08p10444

Materna, K., Bartlow, N., Wech, A., Williams, C. and Bürgmann, R., 2019, Dynamically triggered changes of plate interface coupling in Southern Cascadia: Geophysical Research Letters, v. 46, p. 12890-12899, https://doi.org/10.1029/2019GL084395

Maxson, J.H., 1933, Economic geology of portions of Del Norte and Siskiyou Counties, northwesternmost California: California Journal of Mines and Geology, v. 29, p. 123-160.

McCaffrey, R., Qamar, A.I., King, R.W., Wells, R., Khazaradze, G., Williams, C.A., Stevens, C.W., Vollick, J.J., and Zwick, P.C., 2007, Fault locking, block rotation and crustal deformation in the Pacific Northwest: Geophysical Journal International, v. 169, p. 1315-1340, https://doi.org/10.1111/j.1365-246X.2007.03371.x

Michel, L., Ehlers, T.A., Glotzbach, C., Adams, B.A. and Stübner, K., 2018, Tectonic and glacial contributions to focused exhumation in the Olympic Mountains, Washington, USA: Geology, v. 46, p. 491-494, https://doi.org/10.1130/G39881.1

Mortimer, N. and Coleman, R.G., 1985, A Neogene structural dome in the Klamath Mountains, California and Oregon: Geology, v. 13, p. 253-256, https://doi.org/10.1130/0091-7613(1985)13<253:ANSDIT>2.0.CO;2

Nilsen, T.H., 1984, Tectonics and sedimentation of the Upper Cretaceous Hornbrook Formation, Oregon and California: in Crouch, J. K., and Bachman, S.B., eds., Tectonics and sedimentation along the California margin: Pacific Section S.E.P.M., v. 38, p. 101-118.

Noury, M., Bernet, M., Schildgen, T.F., Simon-Labric, T., Philippon, M., and Sempere, T., 2016, Crustal-scale block tilting during Andean trench-parallel extension: Structural and geo-thermochronological insights: Tectonics, v. 35, p. 2052-2069, https://doi.org/10.1002/2016TC004231

Perttu, R.K., 1976, Structural geology of the northeast quarter of the Dutchman Butte quadrangle, southwest Oregon [M.S. thesis]: Portland State University, 60 p. https://doi.org/10.15760/etd.2439

Pesek, M.E., Perez, N.D., Meigs, A., Rowden, C.C. and Giles, S.M., 2020, Exhumation timing in the Oregon Cascade Range decoupled from deformation, magmatic, and climate patterns: Tectonics, p.e2020TC006078, https://doi.org/10.1029/2020TC006078

Phillips, P.A. and Aalto, K.R., 1989, Tectonically Controlled Basin Development as Indicated by Conglomerates and Other Detritus of the Weaverville Formation, Central and Western Klamath Mountains, Northern California: Pacific Section S.E.P.M., v. 62, p. 81-98.

Piotraschke, R., Cashman, S.M., Furlong, K.P., Kamp, P.J., Danišík, M., and Xu, G., 2015, Unroofing the Klamaths—Blame it on Siletzia?: Lithosphere, v. 7, p. 427-440, https://doi.org/10.1130/L418.1

Puleri, Bryan T., Christensen, Dana J., Davies, Joseph J., Team, Taylor C., Michalak, Melanie J., 2019, New petrologic analysis and thermochronologic constraints on exhumation rate using apatite (U-Th)/He cooling ages of the Granite Peak Pluton, Klamath Mountain Province, NW California: Poster. Geological Society of America Abstracts with Programs, v. 51, no. 4, doi:10.1130/abs/2019CD-329586

Reiners, P.W., Ehlers, T.A., Garver, J.I., Mitchell, S.G., Montgomery, D.R., Vance, J.A. and Nicolescu, S., 2002, Late Miocene exhumation and uplift of the Washington Cascade Range: Geology, v. 30, p. 767-770, https://doi.org/10.1130/0091-7613(2002)030<0767:LMEAUO>2.0.CO;2

Reiners, P.W., Spell, T.L., Nicolescu, S. and Zanetti, K.A., 2004, Zircon (U-Th)/He thermochronometry: He diffusion and comparisons with 40Ar/39Ar dating Geochimica et cosmochimica acta, v. 68, p. 1857-1887, https://doi.org/10.1016/j.gca.2003.10.021

Reiners, P.W. and Brandon, M.T., 2006, Using thermochronology to understand orogenic erosion: Annual Review of Earth and Planetary Sciences, v. 34, p. 419-466, https://doi.org/10.1146/annurev.earth.34.031405.125202

Schmandt, B. and Humphreys, E., 2011, Seismically imaged relict slab from the 55 Ma Siletzia accretion to the northwest United States: Geology, v. 39, p. 175-178, https://doi.org/10.1130/G31558.1

Schmalzle, G.M., McCaffrey, R. and Creager, K.C., 2014, Central Cascadia subduction zone creep: Geochemistry, Geophysics, Geosystems, v. 15, p. 1515-1532, doi:10.1002/2013GC005172

Schultz, K.L., 1983, Paleomagnetism of Jurassic plutons in the central Klamath Mountains, southern Oregon and northern California [M.S. thesis]: Oregon State University, 170 p, https://ir.library.oregonstate.edu/concern/graduate_thesis_or_dissertations/1831cn082

Schweickert, R.A. and Irwin, W.P., 1989, Extensional faulting in southern Klamath Mountains, California: Tectonics, v. 8, p. 135-149, https://doi.org/10.1029/TC008i001p00135

Sliter, W.V., Jones, D.L. and Throckmorton, C.K., 1984. Age and correlation of the Cretaceous Hornbrook Formation, California and Oregon: in Nilsen, T. H., ed., Geology of the Upper Cretaceous Hornbrook Formation, Oregon and California: Pacific Section S.E.P.M., v. 42, p. 89-98.

Stern, R.J. and Dumitru, T.A., 2019, Eocene initiation of the Cascadia subduction zone: A second example of plume-induced subduction initiation?: Geosphere, v. 15, p. 1–23, https://doi.org /10.1130/GES02050.1.

Surpless, K.D. and Beverly, E.J., 2013, Understanding a critical basinal link in Cretaceous Cordilleran paleogeography: Detailed provenance of the Hornbrook Formation, Oregon and California: Geological Society of America Bulletin, v. 125, p. 709-727, https://doi.org/10.1130/B30690.1

Surpless, K.D., 2015, Hornbrook Formation, Oregon and California: A sedimentary record of the Late Cretaceous Sierran magmatic flare-up event: Geosphere, v. 11, p. 1770-1789, https://doi.org/10.1130/GES01186.1

Sutter, J.F., 1978, K-Ar ages of Cenozoic volcanic rocks from the Oregon Cascades west of 121 30': Isochron West, v. 21, p. 15-21.

Team, T., 2018, Cooling and Exhumation History of the Canyon Creek Pluton, Klamath Mountain Province, NW California: [Undergraduate senior thesis] Humboldt, California State University, 46 p.

Vance, J.A., 1984, The lower Western Cascades Volcanic Group in northern California: Pacific Section S.E.P.M., v. 42, p. 195-196.

von Dassow, W., 2018, Geomorphic Evidence for Differential Rock Uplift Across the Southern Cascadia Forearc: [Graduate thesis] Oregon State University, 77 p.

U.S. Geological Survey and ESRI, 2010, plate_lines_and_polygons [dataset] https://www.arcgis.com/home/item.html?id=f155b76c13c84f62864446847f1ae652

U.S. Geological Survey and California Geological Survey, Quaternary fault and fold database for the United States, accessed October 1, 2020, at: https://www.usgs.gov/natural-hazards/earthquake-hazards/faults

Walker, J.D. and Geissman, J.W., 2009, 2009 GSA geologic time scale: GSA Today, v. 19, p. 60-61.

Wells, F.G., 1956, Geology of the Medford quadrangle, Oregon-California: US Geological Survey Geologic Quadrangle Map GQ-89, scale 1:96,000.

Wells, R.E., Weaver, C.S., and Blakely, R.J., 1998, Fore-arc migration in Cascadia and its neotectonic significance: Geology, v. 26, p. 759-762, https://doi.org/10.1130/0091-7613(1998)026<0759:FAMICA>2.3.CO;2

Wells, R., Bukry, D., Friedman, R., Pyle, D., Duncan, R., Haeussler, P., and Wooden, J., 2014, Geologic history of Siletzia, a large igneous province in the Oregon and Washington Coast Range: Correlation to the geomagnetic polarity time scale and implications for a long-lived Yellowstone hotspot: Geosphere, v. 10, p. 692-719, https://doi.org/10.1130/GES01018.1

Yule, J.D., Saleeby, J.B. and Barnes, C.G., 1996, The 175–135 Ma plutons of the Klamath Mountains province reinterpreted as a single oceanic arc batholithic system: Geological Society of America Abstracts with Programs, v. 28, p. 128.